Kara Sea freshwater transport through Vilkitsky Strait: Variability, forcing, and further pathways toward the western Arctic Ocean from a model and observations

M. Janout[1], Y. Aksenov[2], J. Hölemann[1], B. Rabe[1], U. Schauer[1], I. Polyakov[3], S. Bacon[2], A. Coward[2], M. Karcher[1,4], Y.D. Lenn[5], H. Kassens[6], L. Timokhov[7]

[1]Alfred Wegener Institute Helmholtz Centre for Polar and Marine Research, Bremerhaven, Germany

[2]National Oceanography Centre, Southampton, United Kingdom

[3]International Arctic Research Center, Fairbanks, USA

[4]O.A.Sys – Ocean Atmosphere Systems GmbH, Hamburg, Germany

[5]School of Ocean Sciences, Bangor University, Anglesey, United Kingdom

[6]GEOMAR Helmholtz Centre for Ocean Research, Kiel, Germany

[7]Arctic and Antarctic Research Center, St. Petersburg, Russia

Latest update: 25 April 2015

Accepted for publication in the Journal of Geophysical Research

Corresponding author's email: Markus.Janout@awi.de

Abstract

Siberian river water is a first-order contribution to the Arctic freshwater budget, with the Ob, Yenisey, and Lena supplying nearly half of the total surface freshwater flux. However, few details are known regarding where, when and how the freshwater transverses the vast Siberian shelf seas. This paper investigates the mechanism, variability and pathways of the fresh Kara Sea outflow through Vilkitsky Strait towards the Laptev Sea. We utilize a high-resolution ocean model and recent shipboard observations to characterize the freshwater-laden Vilkitsky Strait Current (VSC), and shed new light on the little-studied region between the Kara and Laptev Seas, characterized by harsh ice conditions, contrasting water masses, straits and a large submarine canyon. The VSC is 10-20 km wide, surface-intensified, and varies seasonally (maximum from August-March) and interannually. Average freshwater (volume) transport is 500 ± 120 km^3 a^{-1} (0.53 ± 0.08 Sv), with a baroclinic flow contribution of 50-90%. Interannual transport variability is explained by a storage-release mechanism, where blocking-favorable summer winds hamper the outflow and cause accumulation of freshwater in the Kara Sea. The year following a blocking event is characterized by enhanced transports driven by a baroclinic flow along the coast that is set up by increased freshwater volumes. Eventually, the VSC merges with a slope current and provides a major pathway for Eurasian river water towards the Western Arctic along the Eurasian continental slope. Kara (and Laptev) Sea freshwater transport is not correlated with the Arctic Oscillation, but rather driven by regional summer pressure patterns.

1) Introduction

The Arctic Ocean receives nearly 11% of the earth's river runoff but contains only 1% of the global volume of seawater [Shiklomanov et al., 2000]. The Arctic Ocean surface freshwater flux is a large net input to the ocean, dominated by runoff from North American and Eurasian Rivers [Aagaard and Carmack, 1989, Serreze et al., 2006]. Rivers discharge on the shallow Arctic shelf seas, where different mixing processes produce moderately saline and cold shelf waters. These eventually feed into (and below) the Arctic halocline [Aagaard et al., 1981], insulating the ice cover from the warmer Atlantic-derived waters below. A recent idealized Arctic Ocean model study [Spall, 2013] highlighted the role of freshwater from the Arctic shelves in setting up horizontal salinity gradients across the continental slopes, which, through the dominant impact of salinity on density, are a major driver for the Atlantic water circulation.

The largest freshwater content (FWC) is found in the Canada Basin [Aagaard and Carmack, 1989], where FW accumulates due to Ekman convergence under a predominant anticyclonic atmospheric circulation [Proshutinsky et al., 2009]. FWC varies on interannual and interdecadal time scales [Rabe et al., 2014], which has been linked to large-scale Arctic indices of sea level pressure [Morison et al., 2012; Proshutinsky and Johnson, 1997] and to changes in wind forcing [Giles et al., 2012]. Freshwater budgets, supported by hydrochemical data [Alkire et al., 2010], suggest that ~70% of the Canada Basin's meteoric freshwater must result from Eurasian Rivers [Yamamoto-Kawai et al., 2008; Carmack et al., 2008]. However, the exact pathways and links between the Eurasian shelves and the Canada Basin remain poorly understood.

Nearly 50% of the Arctic river water enters from three of the largest rivers on earth over the vast Kara and Laptev Sea shelves from the Lena (531 $km^3\ a^{-1}$), Ob (412 $km^3\ a^{-1}$), and Yenisey (599 $km^3\ a^{-1}$; Figure 1) [Dai and Trenberth, 2002]. The discharge is highly seasonal (Figure 2) and controls the summer stratification [Janout et al. 2013] and biogeochemical environment on the Siberian shelves [Holmes et al. 2012]. The distribution and fate of the river plumes is primarily dominated by winds in summer [Dmitrenko et al., 2005]. During years with weak or predominantly westerly winds over the Laptev Sea, Lena River water propagates into the East Siberian Sea and further along the coast toward Bering Strait [Weingartner et al., 1999]. During summers with easterly or southerly winds, the plume remains on the central and northern Laptev shelf, and is available for export into the Arctic Basin [Guay et al., 2001].

The Siberian shelves are important ice formation regions. While polynyas are frequent along most of the Laptev and East Siberian coasts, the Kara Sea polynyas are mainly concentrated along the Novaya Zemlya coast and north of Severnaya Zemlya [Winsor and Björk, 2000]. Landfast ice (LFI) can form along the northeast Kara Sea coast as early as in November, and more consistently covers a larger region from February-June [Divine et al., 2004]. Atmospheric conditions considerably affect LFI variability, where the largest extent coincides with high pressure over the Arctic leading to cold offshore winds over the Kara Sea, while cyclones favor a lesser LFI extent and earlier breakup in spring [Divine et al., 2005]. The increasing cyclonicity in the Arctic [Zhang et al., 2004] may in part explain the LFI decrease in the Kara Sea by ~4% decade^{-1} between 1976 and 2007, reported by Yu et al. [2014]. A 5-year model study estimated an average ice volume flux out of the Kara Sea of 220 km^3 a^{-1} [Kern et al., 2005], which is the equivalent of ~200 km^3 of freshwater or ~half of the Ob's annual runoff.

The Kara Sea received considerable attention in the 1980's and 1990's, when circulation and freshwater dispersion studies were designed to predict the fate, residence time, and dilution of nuclear waste deposited in the region, which resulted in a large pool of literature [Pavlov and Pfirman, 1995; Schlosser et al., 1995; Pavlov et al., 1996; Johnson et al., 1997; Harms et al., 2000]. Summer surveys from the 1960's [Hanzlick and Aagaard, 1980] and 1990's [Johnson et al., 1997] observed a northward river plume dispersion during summer. Numerical tracer experiments [Harms et al., 2000] found a similar summer distribution and then a shoreward return of the plume under changing wind directions in the fall. Model results [Harms and Karcher; 1999; Harms and Karcher, 2005; Panteleev et al., 2007], in agreement with previous circulation schemes [Pavlov and Pfirman, 1995; Pavlov et al., 1996], suggest that Vilkitsky Strait (VS) is a prominent pathway for the fresh coastal waters carried within the West Taymyr Current (WTC). The WTC is assumed to wrap around the Taymyr peninsula to continue southward as the East Taymyr Current [Pavlov et al., 1996], which implies that the fresh Kara Sea waters are advected onto the Laptev Sea shelf. However, a detailed Laptev Sea survey from September 2013 suggests that only a small part of the northwestern Laptev Sea shelf is influenced by fresher Kara Sea waters with salinities of ~30 (Figure 3). The provenance of the waters can be determined by dissolved neodymium isotope compositions and preliminary analyses indicate that at least the central Laptev Sea was almost exclusively dominated by Lena River water at that time (G. Laukert, pers. comm.). The comparatively small amount of Kara Sea freshwater on the Laptev Sea shelf may be explained by the region's bathymetry, which is far more complex than previously considered. Immediately eastward of the ~200 m deep VS, the bathymetry deepens into a large submarine canyon (Vilkitsky Trough, VT, see Figure 1). VT is a maximum of 350 m deep, 80 km wide and more than 200 km long [Jakobsson et al., 2008]. Unfortunately, detailed observations and published information from the canyon are missing, which may be primarily due to the harsh ice conditions that often prevail in the region. In a numerical circulation study, Aksenov et al. [2011] mention a fresh current that exits the Kara Sea through VS, and eventually forms the near-surface part of a "pan-arctically persistent current" propagating along the Arctic continental slopes. This proposed pathway of Kara Sea freshwater is contrasted by a propagation along the inner Laptev Sea shelf, and urgently requires observational evidence considering the implications of Siberian freshwater for the Arctic Ocean.

The goal of this study is to shed light on the region between VS and the continental slope along the northern Laptev Sea in order to understand the regional conditions and derive their larger-scale importance for the Arctic Ocean. In particular, we aim to characterize the fresh Kara Sea outflow, investigate its structure, seasonal and interannual variability, and forcing mechanisms based on a high-resolution circulation model combined with recent observations.

The paper is structured as follows. “Data and methods” are provided in section 2. The results section 3 provides a characterization of the Vilkitsky Strait Current (section 3a), associated volume and freshwater transports (section 3b), their variability and forcing mechanisms (section 3c), observations and further pathways (section 3d), and finally the fate of the Kara Sea freshwater (section 3e). The paper finishes with a discussion in section 4 and summary in section 5.

2) Data and methods

a) Model

In this study we analyzed results from an Ocean General Circulation Model (OGCM) developed under the Nucleus for European Modelling of the Ocean (NEMO) framework for ocean climate research and operational oceanography (http://www.nemo-ocean.eu). The NEMO configuration used here is a z-level global coupled sea ice-ocean model, which includes the ocean circulation model OPA9 [Madec et al., 2011] and the Louvain-la-Neuve sea ice model LIM2 [Fichefet and Morales Maqueda, 1997] updated with elastic-viscous-plastic rheology. The ocean model is configured at 1/12 degree on a tri-polar Arakawa C-grid with the model poles at the geographical South Pole, in Siberia and in the Canadian Arctic Archipelago. The nominal horizontal resolution is ~3 km in the area of interest (Kara and Laptev Seas and the eastern Eurasian Basin; Figure 1), 2-4 km in the central Arctic Ocean and Canadian Arctic, and ~9 km in the rest of the ocean. The model is eddy-resolving in the

Arctic Ocean and eddy-permitting on the shelves [Nurser and Bacon, 2014]. The model has 75 vertical levels with 19 levels in the upper 50 m and 25 levels in the upper 100 m. The thickness of top model layer is ~1 m, increasing to ~204 m at 6000 m. Following Barnier et al. [2006], partial steps in the model bottom topography are implemented to improve model approximation of the steep continental slopes. The high vertical resolution and partial bottom steps in topography allow for better simulations of the boundary currents and shelf circulation. The model has a non-linear ocean free surface, improving simulations of the sea surface height. An iso-neutral Laplacian operator is used for lateral tracer diffusion and a bi-Laplacian horizontal operator is applied for momentum diffusion. A turbulent kinetic energy closure scheme is used for vertical mixing [Madec et al., 2011]. The model has been successfully used in several studies of the Arctic Ocean [Lique and Steele, 2012] and the North Atlantic [Bacon et al., 2014]. Amongst the known biases are a ~10% higher than observed sea ice concentration and a 7% higher inflow through Bering Strait [Woodgate et al., 2012].

b) Observations

Conductivity-Temperature-Depth (CTD) measurements from the Laptev Sea originate from several different expeditions. In 2004 and 2005, CTD transects were taken during the NABOS (Nansen and Amundsen Basins Observational System) program aboard the research icebreaker *Kapitan Dranitsyn* using a Seabird 19plus profiler. Accuracies for temperature and conductivity are 0.005°C and 0.0005 Sm^{-1}, respectively. VT sampling in 2011 was carried out during "TRANSARC" aboard *RV Polarstern*, using a Seabird SBE911 CTD with accuracies of 0.001 °C and 0.0003 Sm^{-1} for temperature and salinity, respectively (data published in Schauer et al., [2012]). *Polarstern* operates a 75 kHz vessel-mounted Acoustic Doppler Current Profiler (ADCP), which provides along-track velocity profiles in 8 m bins with an accuracy of 3 cm s^{-1}. In September 2013, the Transdrift-21-expedition to the Laptev Sea was carried out aboard *RV Viktor Buinitskiy* within the framework of the Russian-German "Laptev Sea System"-program. Temperature and salinity transects were carried out using an Ocean Science underway (U-)CTD system, which allows profiling while the ship is in transit. The U-CTD sensors are manufactured by Seabird and provide accuracies of 0.0004 °C and 0.002-0.005 S m^{-1} at a sampling frequency of 16 Hz. The sensors operate in free-fall mode with a non-constant sinking velocity, and subsequent salinity computations require careful alignment of conductivity and temperature samples. The U-CTD post-processing followed the recommendations of Ullmann and Hebert [2014].

3) **Results**

a) Structure, seasonality and pathway of the Vilkitsky Strait Current

A state-of-the-art numerical model (NEMO) with a proven track-record in simulating Arctic Ocean circulation features was investigated for the circulation in the Kara Sea outflow region around VS and the western Laptev Sea (Figure 4). Based on long-term (1990-2010) mean October velocities, the model shows the variable Western Taymyr Current (WTC) in the eastern Kara Sea, which carries western Kara Sea waters mixed with river water along-shore in agreement with Pavlov and Pfirman [1995]. Upon reaching the narrowing strait, the WTC intensifies and continues eastward, first along the southern edge of VT, and then along the continental shelf break of the northern Laptev Sea. In VS, the diffuse WTC develops into a strong and well-defined current, which we henceforth refer to as the Vilkitsky Strait Current (VSC). The VSC is swift and narrow (10-20 km) and propagates eastward along the slopes surrounding the Laptev Sea (Figure 4). During the first 200 km of its propagation along VT the velocities decrease with depth, but increase again once the VSC reached the Laptev continental slope, presumably due to the interaction with other slope currents such as described by Aksenov et al. [2011].

Climatological sections of currents (Figure 5) and salinity (Figure 6) across VS reveal the vertical and horizontal structure and seasonal development of the VSC. Cross-strait velocities show a pronounced surface-intensified jet on the strait's south side, with maximum velocities of >0.5 m s^{-1} during October-December. The jet is ~20 km wide, most intense in the upper 20 m and clearly defined to a depth of 80-100 m from July through March, while it is nearly absent from April – June. The structure of the geostrophic velocities (referenced to the bottom;not shown) computed from the model's density cross-section is identical to that of the current magnitude (Figure 5). Average monthly (0-60m) geostrophic velocities are 10-30% (summer and fall) to 50% (spring) smaller than the total velocities (Figure 7). The baroclinic flow constitutes 70% ± 13% of the currents in VS and implies that the flow is largely buoyancy-driven, which explains the strong coupling of the jets' magnitude and structure to the seasonal freshwater cycle of the Ob and Yenisey (Figure 2) and the cross-strait salinity (Figure 6). Discharge of both rivers peaks in June and subsequently decreases to the minimum runoff rates from November-April (Figure 2). The ~3-month-lag between peak runoff in June and maximum VS velocities in fall may be explained by the time it takes the freshwater to cover the distance of 700-900 km from the rivers' estuaries to VS.

Salinities are markedly lower on the south-side of VS (Figure 6), with minimum values of ~29 from October-January. During this time, across-strait isohalines have the steepest slopes corresponding to maximum velocities. Isohalines level out during spring, when surface salinities are maximum (~31-32), and velocities are minimum. Upper-ocean temperatures in VS (not shown) are near-freezing year-round except from July–September, when the climatological mean reaches ~2 °C on the strait's south side in the core of the VSC. Deeper waters in VS are warmer (>-1 °C) and more saline (34.5-34.8), and influenced by Barents Sea Branch water [Rudels, 2012], which is found in the canyon east of VS as will be shown later.

b) Freshwater and volume transport through Vilkitsky Strait

Transports across VS were quantified based on NEMO results. Volume transport F_{Vol} is computed according to:

$$(1)\ F_{Vol} = \int u dA,$$

where u is the cross-strait velocity and A the area of the strait's cross section. Liquid freshwater transport F_{FW} is estimated using:

$$(2)\ F_{FW} = \int u \times \frac{S_{ref} - S}{S_{ref}} dA,$$

where S is the salinity and a reference salinity S_{ref}=34.80, following Aagaard and Carmack [1989].

Applying (1) and (2) to monthly velocity and salinity from the 21-year simulation results in volume and freshwater transports that strongly resemble each other, as well as a seasonal cycle that is clearly governed by the seasonality in the VSC (Figure 7). Monthly-mean transports are small during spring and early summer, with a minimum in May in volume and freshwater transport of 0.2±0.15 Sv (1 Sv=10^6 m^3 s^{-1}) and 4.8±3.6 mSv, respectively. Transports increase in late summer/early fall to become maximum in December/January, with monthly-mean transports of 0.85±0.30 Sv (26.4±11.8 mSv). The average volume and liquid freshwater transports through VS over 21 years of NEMO simulation are 0.53 ± 0.08 Sv and 497 ± 118 km^3 a^{-1}, respectively.

The mean annual freshwater transport through VS accounts for nearly half of the Kara Sea's annual river runoff, and hence the VSC provides a significant amount of freshwater to the western Laptev Sea shelf and slope region. As shown above, transports vary seasonally with maxima in late fall, but in addition feature considerable interannual variability (Figure 8). The 2-decade-long transport record suggests a volume transport that peaks at 1.5 Sv down-strait, such as in late 2001 and in early 2005 (Figure 8), with occasional reversals (i.e. up-strait transports). In high-flow years, maximum flow in peak transport months can be more than twice the average transport. In low-flow years, maximum flow may only be half as much as the average.

The dominant baroclinic nature of the VSC explains the close resemblance of the volume and freshwater transports (Figure 8) and hence a considerable range in the baroclinic flow fraction. While only ~30% of the flow appears to be baroclinic during low transports in 2004, a baroclinicity of >95% occurs in 2008 and 2009. Overall, the interannual variability in volume and freshwater transport is large enough to play a significant role for the regional and larger-scale freshwater distribution.

c) Interannual transport variability and atmospheric forcing

The transports (Figure 9a) have negative anomalies during several years such as in 1990, 1993, 1998, 2004, and 2010, with values that are up to 0.2 Sv below average for several months. Our modeled salinity/freshwater content anomaly fields during these years shows considerably more freshwater in the western Kara Sea along Novaya Zemlya's east coast, as well as less freshwater in the northeastern Kara Sea along the Taymyr peninsula toward VS in summer and fall (Figure 10). The corresponding Arctic-wide NCEP [Kalnay et al., 1996] sea level pressure patterns and the resulting wind fields over the Kara Sea show anomalously northerly winds during each of these minimum transport periods, often accompanied by enhanced easterly winds (Figure 9b). These conditions favor the advection of river water towards the west, and at the same time a reduction of the VS outflow. These results confirm and expand on a previous study [Harms and Karcher, 2005], which described wind-forced blocking of the VS outflow in 1998 based on a 5-year-long Kara Sea simulation.

Blocking-favorable winds develop under the influence of either a summer high pressure system over the Barents and western Kara Seas and/or a low over the northern Laptev Sea (Figure 9). In the summer after a year with blocking conditions, the runoff gets added to accumulated freshwater and sets up an enhanced northeastward baroclinic flow along the coast in late summer, which may explain why years with negative transport anomalies are followed by years with enhanced volume and freshwater transports (Figures 8 and 9). The residence time for Kara Sea river water is between 2.5 years [Hanzlick and Aagaard, 1980] and 3.5 years [Schlosser et al., 1994], and considering that the annual mean modeled freshwater transport through VS is only ~half of the annual discharge from Ob and Yenisey, the fate of a significant portion of river water remains uncertain. The Kara Sea's only wide opening is to the north between Novaya Zemlya and Severnaya Zemlya, which, based on our results and previous simulations [Panteleev et al., 2007] is bounded by the strong influence of the Barents Sea throughflow (Figure 1b) at least on climatological time scales. For further insights into the Kara Sea-internal conditions during blocking-years, we computed summer volume and freshwater transports across all major Kara Sea openings (Figure 11). Volume transports in particular indicate a larger-scale effect of these blocking situations such as in 1993, 1998 or 2004, when the largest transport reductions of nearly 0.5 Sv occured in the Barents Sea opening and the northern Kara Sea. This is plausible considering that the corresponding pressure systems (Figure 9) favor an Ekman transport against the east- and then northward flow of the Barents Sea outflow. At the same time, the inflow through Kara Gate is reduced. In contrast, both volume and freshwater transports across the opening between Novaya Zemlya and Severnaya Zemlya (Figure 11) are slightly elevated during blocking years, which indicates that ~one-third (e.g. 1993 and 1998) of the negative freshwater transport anomaly exits through the northern Kara Sea instead of VS, while the larger share remains in the Kara Sea. Overall, our simulations largely agree with previous studies [Panteleev et al., 2007] and highlight the importance of the narrow VS as the major Kara Sea freshwater gateway.

The concept of a simple (atmospherically-forced) storage-release mechanism is supported by two hydrographic cross-slope transects across the presumed pathway of the VSC in the northern Laptev Sea along 126°E occupied during the 2004-blocking and 2005-release years (Figures 1 for location; Figure 12). In 2004, salinities above the slope were comparatively high (>30), concurrent with an atmospheric "blocking" pattern and reduced VS model outflow. In the following year, the waters were significantly fresher (~28), representative of enhanced volume and freshwater transports in the simulation.

Meridional summer winds over the eastern Kara Sea appear to influence the variability of volume and freshwater transport through VS. Therefore, we decompose monthly mean reanalyzed SLP from 60-90°N into their principal components by use of empirical orthogonal function (EOF) analysis to identify the dominant modes of variability in Arctic atmospheric patterns and their relation with Siberian shelf processes. The decomposition results in three leading EOF modes, which explain 54.6 %, 12.5 % and 9.1 % of the variance in mean July-September SLP, similar to findings by Overland and Wang [2010]. The first mode is identical to the Arctic Oscillation [Thompson and Wallace, 1998], and describes the strength of the polar vortex. The second highlights the Arctic Dipole Anomaly [Wu et al., 2006], which favors a transpolar circulation from Siberia towards Fram Strait. Both patterns have the largest signals during winter and show no apparent correlation with VS transports. Considering that river discharge and wind-driven currents are maximum in the open water season and when sea ice is thin and mobile, we find that the VS transports best correspond to the third mode (EOF3). This mode is slightly more pronounced during summer (9.1 %) than winter (6.9 %) and describes a pressure pattern centered approximately half-way between the New Siberian Islands and the North Pole (Figure 13), and was previously linked with the freshwater distribution on the Laptev Sea shelf [Dmitrenko et al., 2005; Bauch et al., 2011].

Positive EOF3 patterns within the 1990-2010 simulation period coincide (although not statistically significant) with minimum modeled VS transports (Figures 8 and 9), such as in 1993, 1998, 2004, and 2010. Larger-scale pressure systems are not necessarily stationary and minor shifts may cause different winds in the topographically complex eastern Kara Sea, which may in part explain the weak correlations. Further, average summer winds are weaker and may not prevent the establishment of a predominantly buoyancy-driven outflow with the VSC. The mean summer SLP during anomalously positive patterns highlights a cyclone, which leads to predominantly shoreward winds in the eastern Kara Sea and along-shore winds in the Laptev Sea (Figure 13). Overall, the implications of cyclonic vs. anticyclonic patterns are considerable for the distribution of Lena, Ob and Yenisey waters. Cyclonic conditions block the Kara Sea outflow and favor an eastward removal of Lena water, which enhances the positive salinity anomaly in the northern Laptev Sea (Figure 13), possibly supported by wind-driven onshelf transport of more saline basin water. The opposite occurs during anticyclonic conditions, which enhance the accumulation of freshwater in the northern Laptev Sea due to both a northward diversion of the Lena River plume and an unhampered outflow of fresh Kara Sea waters through VS, likely favoring an export of Siberian river water into the Eurasian Basin.

d) The further pathways and observations in Vilkitsky Trough

Upon exiting VS, the VSC encounters the complex topography of VT with its steep slopes and strong gradients in water mass properties between canyon and Laptev Sea shelf. Along the Laptev shelf-canyon edge, the model features a topographically-guided VSC while the subsurface waters inside the canyon are influenced by recirculating Barents Sea water (not shown). A high-resolution shelf-to-canyon transect was occupied in September 2013 using an underway CTD system (Figure 14). The entire transect is characterized by a sharp halocline, separating the fresh (<31) surface waters from the more saline (>33) waters below 30 m. Surface temperatures are highest (>3°C) on the shelf and low over the slope and canyon, which is likely due to the presence of sea ice in and west of VS at the time of sampling.

The interior canyon waters between 100-250 m feature maximum salinities of 34.8 and temperatures around 0°C, characteristic for the water mass properties that exit the Barents

Sea through the eastern side of St. Anna Trough [Schauer et al., 1997, Schauer et al., 2002, Dmitrenko et al. 2014]. Considering that the Barents Sea waters are transported along the Eurasian slope in the Barents Sea branch [Rudels et al., 1999; Rudels et al., 2000, Aksenov et al. 2011], it is plausible to find that these waters followed the topography into the dynamically-wide VT, where the canyon width of 50-80 km is much larger than the first baroclinic Rossby Radius (~4 km, Nurser and Bacon [2014]).

Near the base of the canyon's slope, isotherms and isohalines become vertical, which translates into a distinct boundary layer at the slope favorable for baroclinic flow. The upper 50-100 m above the slope feature clearly depressed isohalines, which implies the presence of enhanced amounts of freshwater directly above the slope. Geostrophic velocities based on the hydrographic structure imply surface-intensified currents above the shelf edge as well as in a thin boundary layer on the slope. A similar velocity structure was measured with a vessel-mounted ADCP from a cross-canyon transect in September 2011 (Figure 15). Maximum along-canyon velocities of 25 cm s^{-1} were measured over the south-side of VT, suggesting that the southern edge of VT is indeed a region carrying waters that exited the Kara Sea in a surface-enhanced current.

The volume transport through VT at this location amounts to 0.53 Sv, based on a canyon width of 75 km, an average depth of 250 m, and average down-canyon velocities of 0.03 m s^{-1}. This estimate may be low, since the vmADCP misses the strongest flow generally found in the upper 20 m, but provides a first observation-based transport estimate from VT, which is close to NEMO's average VS volume transport. The hydrographic cross-canyon structure from 2011 (Figure 15) is similar to the one measured in 2013, with strong shelf-to-canyon gradients and canyon temperature-salinity-properties that imply Barents Sea origin (34.8, ~0°C). Overall, these observations confirm the existence of a current coming out of the Kara Sea and hence lend support to NEMO's physically plausible suggestions and underline the importance of the VT region for the Eurasian Slope and Basin.

e) On the fate of the Kara Sea freshwater

The fate of ~500 km^3 of freshwater exiting VS per year is clearly of regional importance, but may also impact the larger-scale Arctic freshwater distribution. To investigate the impact of the VSC on the Arctic continental slope currents near the mouth of VT, we extracted three transects from the model domain: 1) upstream; 2) mouth; 3) downstream of VT (Figure 16). The current speed in the "upstream" transect shows a narrow and swift slope-current, with maximum velocities below 100 m and only a weak surface signature. The slope current originates from St. Anna Trough and carries Barents Sea water around the Arctic, and was previously described in detail as the ASBB (Arctic Shelf Break Branch) by Aksenov et al. [2011]. Transect 2 still shows the ASBB as a subsurface feature, and additionally highlights the surface-intensified VSC in the southwestern part of the transect, as it crosses the slope and the outer edge of the northwest Laptev Sea and canyon. Downstream, i.e. east of the canyon mouth (transect 3), the model shows a unified current, which continues along the continental slope as a combination of the near-surface VSC and the sub-surface ASBB. The current now carries Barents Sea branch water at depth and Kara Sea freshwater in the upper layer, reflected by a (0-50 m) freshwater content that is on average ~75% larger in transect 3 compared with transect 1.

Aksenov et al. [2011] previously suggested that nearly 80% of this current propagates along the continental slope into the western Arctic, which (if these results hold in reality) would make it a primary pathway for Siberian river water into the Canada Basin and toward the freshwater storage system of the Beaufort Gyre [Proshutinsky et al., 2009]. The contribution from Eurasian Rivers to the Canada Basin's meteoric freshwater is estimated to be as large as 70% [Yamamoto-Kawai et al., 2008; Carmack et al., 2008], although a clearly defined pathway along the Eurasian slope has not been observed despite numerous expeditions into the Arctic Ocean in the recent decades. One explanation may be that usual sampling strategy in large-scale surveys could easily miss a narrow current such as the one described here. A similar current along the Beaufort Sea slope with horizontal scales of 10-15 km was observed with hydrographic observations [Pickart et al., 2004] and a high-resolution mooring array [Spall et al., 2008; Nikolopoulos et al., 2009], which provides an excellent example for the benefits of finer-scale sampling. The 2013 cross-slope U-CTD transects resolved the shelf break region with a maximum horizontal resolution of 3-6 km near 113°E and 116°E (Figure 14). Both transects resolve a front located in a narrow band between the slopeward edge of the warmer (Barents Sea branch) water and the slope, most pronounced below 100 m depth. Isotherms are vertical in the front, with horizontal temperature gradients of up to 2°C over less than 10 km. These transects highlight a density structure that is favorable for maintaining a geostrophic baroclinic flow along the continental slope as suggested by the model, and underline the need for more modern sampling strategies that allow better resolution of these narrow fronts.

4) Discussion

The aim of this paper is to characterize the VSC including its transports and variability on seasonal and interannual time-scales, and we therefore provide only limited insights into processes that occur on shorter (tides to storms) time scales. On seasonal scales, the VSC is a stable current that (in the model) steadily flows from the origin in VS all the way into the Canada Basin. However, along its path the VSC experiences sudden topographic changes near the mouth of VT (see Figure 1) where it is also exposed to fast-propagating Arctic storms, both conditions which are favorable for generating barotropic and baroclinic instabilities. Instabilities in a buoyant current can generate eddies which may transport some of the Kara Sea freshwater into the Eurasian Basin and potentially modify our conclusions gained in this paper, and should therefore be subject to future investigations.

Sea ice-ocean models including the one used in this study generally do not correctly implement landfast ice (LFI) [Proshutinsky et al., 2007], which might affect certain aspects of the coastal ocean circulation. For instance Itkin et al. [2015] discussed consequences of LFI on brine formation and river water pathways in the Laptev Sea based on a simple LFI parameterization in a regional circulation model. Kasper and Weingartner [2015] investigated the effect of LFI on a river plume along a straight shelf such as the Alaskan Beaufort Sea with an idealized model. They found that introducing LFI enhanced vertical mixing due to frictional coupling between ice and river plume and resulted in a subsurface velocity maximum and a seaward displacement of the plume. Johnson et al. [2012, hereafter J12] implemented LFI in a model by not allowing sea ice to move from November-May in regions shallower than 28 m, and found an ice thickness decrease in parts of the Siberian shelves (most noticeable between the eastern Laptev and the western Chukchi Sea) relative to a control run without LFI. J12 explained their findings by slower (thermodynamic) ice growth because LFI inhibits ice ridging and deformation.

Since significant parts of the northeastern Kara Sea are covered by LFI in winter and spring [Divine et al. 2004], we investigated the previous model results from J12 in more detail in order to obtain qualitative insights regarding the role of LFI on VS transports. We compared the volume and freshwater transports in VS from both experiments (LFI and the control run) described in J12, and found only marginal differences in the volume transports (2% in summer June-October,<1% from December-March). Freshwater transports were 11 ± 7% larger in summer-fall (June-October), and 15 ± 4% smaller in the winter-spring (December-March) with an implementation of LFI, thus the seasonal cycle of the transports is reduced in the LFI simulations. The LFI parameterization in the model inhibited ice export in the Eastern Kara Sea (predominantly north-eastward towards the Nansen Basin in the control run), increasing ice divergence and open water at the outer LFI edge. The effect of the LFI parameterization was such that ice production and salt fluxes in winter and spring were moderately reduced near the LFI-covered coast, but greatly enhanced at the outer LFI edge, thus overall reducing VS freshwater transport in the LFI run. While we cannot necessarily expect a realistic representation of LFI with a simple parameterization, this comparison indicates that the absence of LFI on the southern Kara and Laptev Sea shelves moderately increases the uncertainty in our results, although it is not detrimental for the presented conclusions. A more physical representation of LFI should be considered in future model studies.

Tides are not implemented in our study, and although tides are generally small in the Arctic [Padman and Erofeeva, 2004], some shelf regions such as the Laptev Sea feature substantial tidal currents with the potential to increase vertical mixing [Janout and Lenn, 2014]. A similar conclusion is reached by model studies regarding the role of tides on Arctic hydrographic properties [Luneva et al., 2015], which found indications for enhanced tide-induced mixing manifested by colder and fresher bottom waters in parts of the Kara Sea. However, tidal currents are weak along the northeastern Kara Sea coast and the VSC pathway in VT [Padman and Erofeeva, 2004] and north of the Laptev Sea [Pnyushkov and Polyakov, 2011] and likely would not noticeably affect the properties of the VSC. Therefore, we expect that our conclusions regarding the pathway of the VSC and the Siberian freshwater are not substantially biased by neglecting the tides.

Our results suggest that a considerable portion of the Kara Sea freshwater enters the Laptev Sea and Eurasian continental slope region in a pronounced surface-intensified current, which strongly varies on seasonal and interannual time scales. The estimated ~500 km^3 a^{-1} only account for the liquid freshwater portion, while an additional part of the Kara Sea freshwater may leave the shelf as sea ice. However, the Siberian shelves are vast and often ice-free during recent summers. Satellite-based studies showed that sea ice formed in the river plume near the Lena Delta region is not exported into the Basin but rather melts on the shelf [Krumpen et al., 2013], which supports the assumption that the majority of freshwater is exported in its liquid phase, at least in the Laptev Sea. Mean model-based Kara Sea ice export estimates are 220 $km^3\ a^{-1}$ [Kern et al., 2005], although the recent advances to remotely sense sea ice thickness may allow more robust ice volume fluxes in the future.

The VS freshwater transport alone, computed as the freshwater anomaly relative to a salinity of 34.8 [Aagaard and Carmack, 1989], comprises ~30% of the Pacific freshwater inflow through Bering Strait [Woodgate et al., 2012]. However, our estimate is low since additional smaller export pathways through the Severnaya Zemlya islands as well as sea ice export were not considered. Further, the model uses climatological mean river discharge [Dai and Trenberth, 2002] and does not consider observed trends or interannual variability in runoff [Peterson et al., 2002]. These, however, are small (O(10%)) compared with the atmospherically-controlled VS freshwater transport variability (O(50%)). The Kara Sea outflow is regulated by pressure patterns that may simultaneously affect the distribution of the Laptev Sea freshwater. Figures 9 and 13 indicate that onshore winds in the Kara Sea block the VS outflow, while along-shore winds near the Lena Delta export freshwater into the East Siberian Sea. This implies that larger-scale pressure systems during summer may primarily control the distribution and fate of three of the earth's largest rivers. Morison et al. [2012] observed an increase in Canadian Basin freshwater along with a decrease in Eurasian Basin freshwater, which they attributed to alterations in the pathways of Siberian river runoff under varying AO conditions. Similarly, Steele and Ermold [2004] linked decadal salinity trends on the Siberian shelves to the AO. Panteleev et al. [2007] related moderately elevated VS transports in their assimilation model to anomalous westerly winds over the Kara Sea prevalent during positive summer AO conditions. In contrast, the interannual variability in Arctic Ocean freshwater storage in recent decades does not noticeably relate to the AO, but rather corresponds to changes in regional wind and ocean circulation [Rabe et al., 2014]. Similarly, our VS transports show no obvious relationship with summer or winter AO, which indicates that, as earlier studies suggest [Bauch et al., 2011], regional conditions dominate the Siberian freshwater pathways.

The open water season is crucial in shaping the hydrographic conditions, as this is the time of the year of maximum river discharge, baroclinic flows develop, and wind stress imparts advection and vertical mixing. The recent years were characterized by freeze-ups that were delayed well into October, which leaves the ocean under a prolonged and stronger influence of fall storms. A continuation of this trend might potentially alter the predominantly baroclinic structure of the VSC and enhance synoptic-scale horizontal and vertical freshwater dispersion, which makes the pathways and distribution of Siberian freshwater depending more on the local variability of the wind patterns and less on the continental freshwater discharge.

5) Summary and conclusion

This paper characterizes the Vilkitsky Strait Current (VSC) including its volume and freshwater transports and their seasonal and interannual variability based on a well-resolved (~3 km) numerical model (NEMO) complemented by recent shipboard observations. The surface-intensified 10-20 km-wide VSC is the continuation of the variable West Taymyr Current in the eastern Kara Sea and the primary pathway to carry river runoff from the Kara Sea through Vilkitsky Strait (VS) and subsequently along Vilkitsky Trough (VT) and the continental slope along the Laptev Sea (Figure 4). Some recent shipboard surveys from VT across the presumed VSC pathway qualitatively confirm the existence of enhanced flow and lower salinity waters over the southern canyon slope (Figures 14 and 15), although a direct comparison with model results is not possible due to non-overlapping time periods. The VSC is strongest during October-March and nearly recedes from April-July (Figures 5-7), with annual mean volume and freshwater transports of 0.53 ± 0.08 Sv and 497 ± 118 km a^{-1}, respectively, based on a 21 year simulation. The VSC is predominantly buoyancy-driven, with a fraction of baroclinic to total flow that varies from ~50% in spring to ~90% in fall.

Strong interannual VSC transport variability is explained by a storage-release mechanism, which is dominated by atmospheric pressure patterns during summer (Figures 9 and 13), when winds have the maximum impact on the river plume distribution. Minimum transports occur, when northerly or northeasterly winds due to a low pressure system north of the Laptev Sea prevent the along-coast spreading of freshwater and block the outflow through VS. The blocking accumulates freshwater on the shelf, which is then released in the following year when the next pulse of runoff gets added and sets up an along-shore baroclinic flow toward VS. The same pattern causes westerly winds over the Laptev Sea, which then favors the removal of Lena water towards the East Siberian Sea, and overall strengthens a positive salinity anomaly in the northern Laptev Sea (Figure 13).

The model suggests that upon arrival at the canyon mouth, the VSC merges with the Barents Sea Branch of the Arctic Boundary Current (Figure 16), and subsequently follows the Eurasian continental slope into the Canadian Basin. The interaction between these two baroclinic currents is not understood and requires a closer investigation. If these results hold, the VSC would be a primary pathway for Siberian river water towards the Beaufort Gyre freshwater storage system, and would hence impact Arctic freshwater distribution. Our conclusions here are mainly based on long-term mean model results. These are qualitatively supported by the few observations that exist from this region that is characterized by complex bathymetry (straits, submarine canyon, steep slopes), multiple contrasting water masses, difficult sea ice conditions, and the largest river discharge to be found in the Arctic. The measurements presented in this paper underline the need for modern sampling strategies to better resolve fronts and baroclinic currents, regional features that occur on small enough scales to be missed by classic large-scale surveys, but which may explain missing links in the Arctic Ocean system.

Clearly, further steps have to be taken to investigate the stability of the VSC and associated freshwater fluxes to obtain more reliable budgets and, perhaps more importantly, to identify “hotspots”, where eddy fluxes export the shelves’ freshwater to the Arctic interior. Eddy fluxes are assumed to supply the Arctic halocline waters as well as to provide the potential energy needed to drive the cyclonic boundary current [Spall, 2013], and the only way to investigate these further is by use of high-resolution numerical models, ideally supported by high-resolution year-round measurements.

6) Acknowledgements

Financial support for the Laptev Sea System project was provided by the German Federal Ministry of Education and Research (Grant BMBF 03G0759B and 03G0833B) and the Ministry of Education and Science of the Russian Federation. The 2011 CTD and ADCP data are available at http://www.pangea.de. NABOS data are available at http://nabos.iarc.uaf.edu. NCEP Reanalysis data were provided by the NOAA-CIRES Climate Diagnostics Center, Boulder, CO, USA, from their Web site at http://www.cdc.noaa.gov/. Data from the 2013 CTD survey as well as the model results will be made available by the authors upon request (markus.janout@awi.de). River discharge data was downloaded from the Arctic RIMS website (http://rims.unh.edu/data.shtml). The study is also a contribution to the TEA-COSI Project of the UK Arctic Research Programme (NERC grant number NE/I028947/), The UK Natural Environment Research Council (NERC) Marine Centres' Strategic Research Programme. We thank the Forum for Arctic Ocean Modeling and Observational Synthesis (FAMOS), funded by the National Science Foundation Office of Polar Programs (awards PLR-1313614 and PLR-1203720), for providing an opportunity to discuss the presented ideas at the FAMOS meetings. The NOCS-ORCA simulations were completed as part of the DRAKKAR collaboration (Barnier et al. 2006). NOC also acknowledges the use of UK National High Performance Computing Resource. We thank the crews and captains of the various research vessels involved in generating the observations. We sincerely acknowledge the thorough comments from the editor (A. Proshutinsky) and two anonymous reviewers, which helped to improve the manuscript.

7) **References**

Aagaard, K., L. K. Coachman, and E. C. Carmack (1981), On the halocline of the Arctic Ocean, *Deep-Sea Res.*, 28, 529– 545.

Aagaard, K., *and* E. C. Carmack (1989), The role of sea ice and other fresh water in the Arctic circulation, *J. Geophys. Res*., 94*(*C10*)*, 14485–14498*, doi:*10.1029/JC094iC10p14485.

Aksenov, Y., V. V. Ivanov, A. J. G. Nurser, S. Bacon, I. V. Polyakov, A. C. Coward, A. C. Naveira-Garabato, and A. Beszczynska-Moeller (2011), The Arctic Circumpolar Boundary Current, *J. Geophys. Res.*, 116, C09017, doi:10.1029/2010JC006637.

Alkire, M.B., K.K. Falkner, J. Morison, R.W. Collier, C.K. Guay, R.A. Desiderio, I.G. Rigor, and M. McPhee (2010), Sensor-based profiles of the NO parameter in the central Arctic and southern Canada Basin: New insights regarding the cold halocline, *Deep-Sea Res. I*, 57, 1432-1443, doi:10.1016/j.dsr.2010.07.011.

Bacon, S., A. Marshall, N. P. Holliday, Y.Aksenov, and S. R. Dye (2014), Seasonal variability of the East Greenland Coastal Current, *J. Geophys. Res. Oceans*, 119 , 3967–3987, doi:10.1002/2013JC009279.

Barnier, B., G. Madec, T. Penduff, J-M. Molines, A.-M. Treguier, J. Le Sommer, A. Beckmann, A. Biastoch, C. Böning, J. Dengg, C. Derval, E. Durand, S. Gulev, E. Remy, C. Talandier, S. Theetten, M. Maltrud, J. McClean, and B.A. de Cuevas B (2006), Impact of partial steps and momentum advection schemes in a global ocean circulation model at eddy permitting resolution, *Ocean Dyn*., 56, 543-567.

Bauch, D., M. Gröger, I. Dmitrenko, J. Hölemann, S. Kirillov, A. Mackensen, E. Taldenkova, and N. Andersen (2011), Atmospheric controlled freshwater release at the Laptev Sea continental margin, *Polar Res.*, 30, 1–14, doi:10.3402/polar.v30i0.5858.

Carmack, E., McLaughlin, F., Yamamoto-Kawai, M., Itoh, M., Shimada, K., Krishfield, R., Proshutinsky, A. (2008), Freshwater storage in the Northern Ocean and the special role of the Beaufort Gyre. In: Dickson, R.R., Meincke, J., Rhines, P. (Eds.), Arctic-Subarctic Ocean Fluxes: Defining the Role of the Northern Seas in Climate. Springer, pp. 145–170.

Dai, A., K.E. Trenberth (2002), Estimates of freshwater discharge from continents: latitudinal and seasonal variations, *J. Hydrometeorol.*, 3, 660-687.

Divine, D. V., R. Korsnes, and A. P. Makshtas (2004), Temporal and spatial variation of shore-fast ice in the Kara Sea, *Cont. Shelf Res.*, 24, 1717–1736, doi:10.1016/j.csr.2004.05.010.

Divine, D. V., R. Korsnes, A. P. Makshtas, F. Godtliebsen, and H. Svendsen (2005), Atmospheric-driven state transfer of shore-fast ice in the northeastern Kara Sea, *J. Geophys. Res.*, 110, C09013, doi:10.1029/2004JC002706.

Dmitrenko, I., Kirillov, S., Eicken, H., Markova, N. (2005), Wind-driven summer surface hydrography of the eastern Siberian shelf, *Geophys. Res. Lett.*, 32. doi:10.1029/2005GL023022.

Dmitrenko, I. A., S.A. Kirillov, N. Serra, N.V. Koldunov, V.V. Ivanov, U. Schauer, I.V. Polyakov, D. Barber, M.A. Janout, V.S. Lien, M. Makhotin, and Y. Aksenov (2014), Heat loss from the Atlantic water layer in the northern Kara Sea: causes and consequences, *Ocean Sci.*, 10, 719-730, doi:10.5194/os-10-719-2014.

Fichefet, T., and M. A. Morales Maqueda (1997), Sensitivity of a global sea ice model to the treatment of ice thermodynamics and dynamics, *J. Geophys. Res*., 102(C6), 12609–12646.

Giles, K. A., S. W. Laxon, A. L. Ridout, D. J. Wingham, and S. Bacon (2012), Western Arctic Ocean freshwater storage increased by wind-driven spin-up of the Beaufort Gyre, *Nat. Geosci*., *5*, 194–197, doi:10.1038/ngeo1379.

Guay, C.K., R.D. Falkner, R.D. Muench, M. Mensch, M. Frank, and R. Bayer (2001), Wind-driven transport pathways for Eurasian Arctic river discharge, *J. Geophys. Res.*, 106, 11,469-11,480.

Hanzlick, D., and K. Aagaard (1980), Freshwater and Atlantic Water in the Kara Sea, *J. Geophys. Res.,* 85 (C9), 4937–4942.

Harms, I. H., and M. J. Karcher (1999), Modeling the seasonal variability of hydrography and circulation in the Kara Sea, *J. Geophys. Res.*, 104(C6), 13,431–13,448.

Harms, I. H., M. J. Karcher, and D. Dethleff (2000), Modelling Siberian river runoff - Implications for contaminant transport in the Arctic Ocean, *J. Mar. Syst.*, 27, 95– 115.

Harms, I. H., and M. J. Karcher (2005), Kara Sea freshwater dispersion and export in the late 1990s, *J. Geophys. Res*., 110, C08007, doi:10.1029/ 2004JC002744.

Holmes, R. M., *et al*. *(*2011*)*, Seasonal and annual fluxes of nutrients and organic matter from large rivers to the Arctic Ocean and surrounding seas, *Estuaries Coasts*, *doi:*10.1007/s12237-011-9386-6.

Itkin, P., M. Losch, and R. Gerdes (2015), Landfast ice affects the stability of the Arctic halocline: Evidence from a numerical model, *J. Geophys. Res. Oceans*, 120, doi:10.1002/2014JC010353.

Jakobsson, M., R. Macnab, L. Mayer, R. Anderson, M. Edwards, J. Hatzky, H. W. Schenke, and P. Johnson (2008), An improved bathymetric portrayal of the Arctic Ocean: Implications for ocean modeling and geological, geophysical and oceanographic analyses. *Geophys. Res. Lett.*, doi: 10.1029/2008gl033520.

Janout, M. A., J. Hölemann, and T. Krumpen (2013), Cross-shelf transport of warm and saline water in response to sea ice drift on the Laptev Sea shelf, *J. Geophys. Res. Oceans*, 118, 563–576, doi:10.1029/2011JC007731.

Janout, M.A.,and Y.D. Lenn (2014), Semidiurnal tides on the Laptev Sea Shelf based on oceanographic moorings with implications for shear and vertical mixing, *J. Phys. Oceanogr.*, 44 (1), 202-219, doi: 10.1175/JPO-D-12-0240.1.

Johnson, D.R., T.A. McClimans, S. King, Ø. Grenness (1997), Fresh water masses in the Kara Sea during summer, *J. Mar. Syst.*, 12, 127– 45.

Johnson, M., et al. (2012), Evaluation of Arctic sea ice thickness simulated by Arctic Ocean Model Intercomparison Project models, J. Geophys. Res., 117, C00D13, doi:10.1029/2011JC007257.

Kalnay, E., et al. (1996), The NCEP/NCAR 40-year reanalysis project. *Bull. Amer. Meteor. Soc.*, 77, 437471.

Kasper, J.L. and T. J. Weingartner (2015), The Spreading of a Buoyant Plume Beneath a Landfast Ice Cover, *J. Phys. Oceanogr.*, 45, 478–494, doi: 10.1175/JPO-D-14-0101.1.

Kern, S., I. Harms, S. Bakan, and Y. Chen (2005), A comprehensive view of Kara Sea polynya dynamics, sea-ice compactness and export from model and remote sensing data, *Geophys. Res. Lett.*, 32, L15501, doi:10.1029/2005GL023532.

Krumpen T., M.A. Janout, K.I. Hodges, R. Gerdes, F. Ardhuin, J.A. Hoelemann, S. Willmes (2013), Variability and trends in Laptev Sea ice outflow between 1992-2011, *Cryosphere*, 7(1), 349-363.

Lique, C., and M. Steele (2012), Where can we find a seasonal cycle of the Atlantic water temperature within the Arctic Basin?, *J. Geophys. Res.*, 117 , C03026, doi:10.1029/2011JC007612.

Luneva M., Y. Aksenov, J.D. Harle, J. T. Holt, The effects of tides on the water mass mixing and sea ice in the Arctic Ocean, *J. Geophys. Res.*, under review.

Madec, G., and the NEMO team (2011), NEMO ocean engine, version 3.2, Note du Pole de modelisation de l'Institut Pierre-Simon Laplace No 27, ISSN No 1288-1619.

Morison, J., R. Kwok, C. Peralta-Ferriz, M. Alkire, I. Rigor, R. Andersen, and M. Steele (2012), Changing Arctic Ocean freshwater pathways, *Nature*, *481*, 66–70, doi:10.1038/nature10705.

Nikolopoulos, A., R. S. Pickart, P. S. Fratantoni, K. Shimada, D. J. Torres, and E. P. Jones (2009), The western Arctic boundary current at 152°W: Structure, variability, and transport, *Deep Sea Res., Part II*, 56, 1164 1181, doi:10.1016/j.dsr2.2008.10.014.

Nurser, A. J. G. and Bacon, S. (2014), The Rossby radius in the Arctic Ocean, *Ocean Sci.*, 10, 967-975, doi:10.5194/os-10-967-2014.

Overland, J. E., and M. Wang (2010), Large-scale atmospheric circulation changes are associated with the recent loss of Arctic sea ice, *Tellus*, Ser. A, 62, 1–9, doi:10.1111/j.1600-0870.2009.00421.x.

Panteleev, G., A. Proshutinsky, M. Kulakov, D. A. Nechaev, and W. Maslowski (2007), Investigation of the summer Kara Sea circulation employing a variational data assimilation technique, *J. Geophys. Res.*, 112, C04S15, oi:10.1029/2006JC003728.

Pavlov, V. K., and S. I. Pfirman (1995), Hydrographic structure and variability of the Kara Sea: Implication for pollutant distribution, *Deep Sea Res. II*, 42, 1369– 1390.

Pavlov, V. K., L. A. Timokhov, G. A. Baskakov, M. Y. Kulakov, V. K. Kurazhov, P. V. Pavlov, S. V. Pivovoarov, and V. V. Stanovoy (1996), Hydrometeorological regime of the Kara, Laptev, and East-Siberian Seas, *Tech. Memo. APL-UW TM* 1-96, 179 pp., Appl. Phys. Lab., Univ. of Wash., Seattle.

Padman, L., and S. Erofeeva (2004), A barotropic inverse tidal model for the Arctic Ocean. *Geophys. Res. Lett.*, 31, L02303, doi:10.1029/2003GL019003.

Peterson, B. J., R. M. Holmes, J. W. McClelland, C. J. Vörösmarty, R. B. Lammers, A. I. Shiklomanov, I. A. Shiklomanov, and S. Rahmstorf (2002), Increasing river discharge to the Arctic Ocean, *Science,* 298**,** 2171–2173.

Pickart, R. S. (2004), Shelfbreak circulation in the Alaskan Beaufort Sea: Mean structure and variability, *J. Geophys. Res.*, 109, C04024, doi:10.1029/2003JC001912.

Pnyushkov, A.V. and I.V. Polyakov (2012), Observations of Tidally Induced Currents over the Continental Slope of the Laptev Sea, Arctic Ocean, *J. Phys. Oceanogr.*, 42, 78–94.

Proshutinksy, A. Y., and M. A. Johnson (1997), Two circulation regimes of the wind-driven Arctic Ocean, *J. Geophys. Res.*, *102*, 12,493–12,514.

Proshutinsky, A., I. Ashik, S. Häkkinen, E. Hunke, R. Krishfield, M. Maltrud, W. Maslowski, *and* J. Zhang *(*2007*)*, Sea level variability in the Arctic Ocean from AOMIP models, *J. Geophys. Res.*, 112, *C04S08, doi:*10.1029/2006JC003916.

Proshutinsky, A., R. Krishfield, M.-L. Timmermans, J. Toole, E. Carmack, F. McLaughlin, W. J. Williams, S. Zimmermann, M. Itoh, and K. Shimada (2009), Beaufort Gyre freshwater reservoir: State and variability from observations, *J. Geophys. Res.*, *114*, C00A10, doi:10.1029/2008JC005104.

Rabe, B., M. Karcher, F. Kauker, U. Schauer, J. M. Toole, R. A. Krishfield, S. Pisarev, T. Kikuchi, and J. Su (2014), Arctic Ocean basin liquid freshwater storage trend 1992–2012, *Geophys. Res. Lett.*, *41*, 961–968, doi:10.1002/2013GL058121.

Rudels, B., Friedrich, H. J., and Quadfasel, D. (1999), The Arctic Circumpolar Boundary Current, *Deep-Sea Res.* II, 46, 1023–1062.

Rudels, B., Muench, R.D., Gunn, J., Schauer, U., Friedrich, H.J. (2000), Evolution of the Arctic Ocean boundary current north of the Siberian shelves, *J. Mar. Syst.*, 25, 77–99.

Rudels, B. (2012), Arctic Ocean circulation and variability – advection and external forcing encounter constraints and local processes, *Ocean Sci.*, 8, 261-286.

Schauer, U., Muench, R.D., Rudels, B., Timokhov, L. (1997), The impact of eastern Arctic Shelf Waters on the Nansen Basin intermediate layers. *J. Geophys. Res.*,102, 3371–3382.

Schauer, U., H. Loeng, B. Rudels, V.K. Ozhigin, and W. Dieck (2002), Atlantic Water flow through the Barents and Kara Seas, *Deep Sea Res. I, 49*, 2281–2298.

Schauer, U., Rabe, B., Wisotzki, A. (2012), Physical oceanography during POLARSTERN cruise ARK-XXVI/3. *Alfred Wegener Institute, Helmholtz Center for Polar and Marine Research, Bremerhaven*, doi:10.1594/PANGAEA.774181.

Schlosser, P., D. Bauch, R. Fairbanks and G. Bönisch (1994), Arctic river runoff: mean residence time on the shelves and in the halocline, *Deep-Sea Res. I, 41, 1053-1068.*

Schlosser, P., J.H. Swift, D. Lewis, and S. Pfirman (1995), The role of the large-scale Arctic Ocean circulation in the transport of Contaminants, *Deep-Sea Res. II*, 42 (6), pp. 1341-1367.

Shiklomanov, I. A., A. I. Shiklomanov, R. B. Lammers, B. J. Peterson, and A. J. Vorosmarty (2000), The dynamics of river water inflow to the Arctic Ocean, in *Fresh Water budget of the Arctic Ocean* , edited by E. L. Lewis, pp. 281–296, Kluwer Acad., Norwell, Mass.

Serreze, M. C., A. P. Barrett, A. G. Slater, R. A. Woodgate, K. Aagaard, R. B. Lammers, M. Steele, R. Moritz, M. Meredith, and C. M. Lee (2006), The large-scale freshwater cycle of the Arctic, *J. Geophys. Res.*, *111*, C11010, doi:10.1029/2005JC003424.

Spall, M. A., R. S. Pickart, P. Fratantoni, and A. Plueddemann (2008), Western Arctic shelfbreak eddies: Formation and transport, *J. Phys. Oceanogr.*, 38, 1644– 1668.

Spall, M. A. (2013), On the circulation of Atlantic Water in the Arctic Ocean, *J. Phys. Oceanogr.*, 43, 2352–2371, doi:10.1175/JPO-D-13-079.1.

Steele, M., and W. Ermold (2004), Salinity trends on the Siberian Shelves, *Geophys. Res. Lett.*, 31, L24308, doi:10.1029/2004GL021302.

Thompson, D.W.J., and J.M. Wallace (1998), The Arctic Oscillation signature in the wintertime geopotential height and temperature fields, *Geophys.Res. Lett*., 25, doi: 10.1029/98GL00950

Ullman, D.S., and D. Hebert (2014), Processing of Underway CTD Data, *J. Atmos. Oceanic Technol.*, 31, 984–998, doi: /10.1175/JTECH-D-13-00200.1

Weingartner, T. J., S. Danielson, Y. Sasaki, V. Pavlov, and M. Kulakov (1999), The Siberian coastal current: A wind- and buoyancy-forced Arctic coastal current, *J. Geophys. Res.*, 104, 29,697– 29,714.

Winsor, P., and G. Björk (2000), Polynya activity in the Arctic Ocean from 1958 to 1997, *J. Geophys. Res.*, 105(C4), 8789–8803, doi:10.1029/1999JC900305.

Woodgate, R. A., T. J. Weingartner, and R. Lindsay (2012), Observed increases in Bering Strait oceanic fluxes from the Pacific to the Arctic from 2001 to 2011 and their impacts on the Arctic Ocean water column, *Geophys. Res. Lett.*, *39*, L24603, doi:10.1029/2012GL054092.

Wu, B., J. Wang, and J. E. Walsh (2006), Dipole anomaly in the winter Arctic atmosphere and its association with sea ice motion, *J. Climate*, 19, 210-225.

Yamamoto-Kawai, M., F. A. McLaughlin, E. C. Carmack, S. Nishino, and K. Shimada (2008), Freshwater budget of the Canada Basin, Arctic Ocean, from salinity, d18O, and nutrients, *J. Geophys. Res.*, 113, C01007, doi:10.1029/2006JC003858.

Yu, Y., H. Stern, C. Fowler, F. Fetterer, and J. Maslanik (2014), Interannual variability of Arctic landfast ice between 1976 and 2007, *J. Clim.*, 27, 227–243, doi:10.1175/JCLI-D-13–00178.1.

Zhang, X., J. Walsh, U. Bhatt, and M. Ikeda (2004), Climatology and interannual variability of Arctic cyclone activity: 1948–2002, *J. Clim.*, 17, 2300–2317.

8) Figure captions

Figure 1: a) Map of the Arctic Ocean, the dark shading highlights the shallow shelf areas (<200 m), the box indicates the boundaries of panel b) map of the Kara and Laptev Seas region. Shading separates depths deeper (grey) and shallower (white) than 200 m from the International Bathymetric Chart of the Arctic Ocean (Jakobsson et al., 2008). c) zoom into the Vilkitsky Strait (VS) and Trough (VT) region. Colored lines and dots show transect locations: VS model-transect (magenta), *RV Polarstern* 2011 VT-transect (blue dots), 2013 UCTD-transect along 113°E and 116°E (red dots), and the 126°E-NABOS-transect (blue line).

Figure 2: Monthly climatological river discharge rates (m^3 s^{-1}) from the three largest Siberian rivers, computed from ArcticRIMS runoff data from 1936-2000 including the standard deviations for Lena and Yenisey.

Figure 3: Mean surface (0-10 m) salinity in September 2013 sampled with an Underway CTD during Transdrift 21. Note that all salinity values are capped below 21 and above 33, minimum salinities were as low as 6 psu near the Lena Delta. The dominant freshwater sources are indicated with blue arrows (Lena and Khatanga Rivers, as well as the Kara Sea outflow). Depth contours show the 20 m, 50 m, 100 m, 200 m, and 1000 m isobaths. The dashed line in the northwest Laptev Sea indicates a boundary between Kara Sea waters in the northwest, and Lena waters based on salinity and neodymium measurements (G. Laukert, unpublished data).

Figure 4: Mean (1990-2010) October a) surface and b) 70 m current speed from NEMO (m s^{-1}).

Figure 5: Monthly mean velocities across Vilkitsky Strait versus depth from NEMO (1990-2010). The right-hand of the transect (km 0) is the south side (i.e. the Laptev Sea side), flow toward the Laptev Sea is into the page. Black dots in November-panel indicate model grid points (see Figure 1 for location).

Figure 6: Same as Figure 5 except for salinity.

Figure 7: Monthly mean (top) volume (Sv) and freshwater (km^3 $month^{-1}$) transport through Vilkitsky Strait from NEMO (1990-2010) and (bottom) mean (0-60 m) total (black) and geostrophic velocities (grey) computed from the NEMO density structure. Vertical bars denote one standard deviation.

Figure 8: Model-based: (a) annual means of volume (blue, [Sv]) and freshwater transport (red, [km^3 $year^{-1}$]). (b) monthly mean volume (blue) and freshwater (red) transports. (c) baroclinic flow fraction in Vilkitsky Strait, i.e. the fraction of geostrophic vs the total velocities in the upper 60 m.

Figure 9: a) Volume transport anomaly through Vilkitsky Strait based on NEMO 1990-2010, x-ticks mark January of each year. (b) NCEP summer wind components over the eastern Kara Sea (white star in panel ”1993”, averaged from July-September. (c) principal components from the third leading EOF decomposed from JAS sea level pressure (60-90 °N). (d) Summer (JAS) SLP distribution during years characterized by strong negative transport anomalies through Vilkitsky Strait, indicated by green stars in the middle panel.

Figure 10: Maps of simulated Kara Sea freshwater content difference (m) between the summers of : a)1993 minus 1994; b) 1998 minus 1999; and c) 2004 minus 2005.

Figure 11: a) Volume (Sv) and b) freshwater (mSv) transport anomalies from NEMO computed from June-October averages across all major Kara Sea gateways. The colors indicate the boundaries as shown in the small map (blue: Vilkitsky Strait; green: Kara Gate; red: Franz Josef Land (FJL) to Novaya Zemlya (NZ); black: FJL to Severnaya Zemlya (SZ); magenta: Shokalsky Strait; cyan: NZ to SZ.

Figure 12: NABOS salinity transects along 126 °E during the summers of 2004 (left) and 2005 (right). Note the comparatively high salinity (low salinity) in 2004 (2005) during negative (positive) freshwater transport anomalies in Vilkitsky Strait. See map Figure 1 for location.

Figure 13: top) The black contours indicate the third largest mode of variability, based on an EOF analysis of Arctic Ocean (latitude >60°N) summer (JAS) NCEP sea level pressure from 1948-2013. This pattern corresponds to a blocking situation of the VSC due to onshore winds (indicated by arrows) over the eastern Kara Sea leading to negative anomalies in Vilkitsky Strait volume and freshwater transport. At the same time, winds are zonal over the southern Laptev Sea, leading to an eastward diversion of the Lena River plume. Overall, this situation leads to positive salinity anomalies in the Laptev Sea, as indicated by the red “S+” - boxes, and to negative salinity anomalies in the Kara and the East Siberian Seas.

Figure 14: Cross-slope temperature (°C; a, c) and salinity (b, d) underway-CTD transects from September 2013 along 113 °E (a, b) and 116 °E (c, d) (see map for location) versus distance (km). Dots at the bottom of the panels indicate station locations.

Figure 15: Figure 15: Cross-canyon CTD and vmADCP transect carried out by *RV Polarstern* in September 2011. a) salinity, b) temperature (°C) overlaid by density contours (kg m^{-3}), c) vessel-mounted ADCP velocity (ms^{-1}, positive eastward); small insert map in b) shows the

location of CTD stations (blue dots) and ADCP transect (red line). Black dots in a) and b) indicate station locations. The black shading indicates the along-track bottom topography, extracted from IBCAO (Jakobbson et al., 2008).

Figure 16: Current speed (m s^{-1}) in three model-based example transects from January 2004 showing the merging of the Barents Sea branch with the Vilkitsky Strait Current. Lower panel shows the location of the three transects.

9) Figures

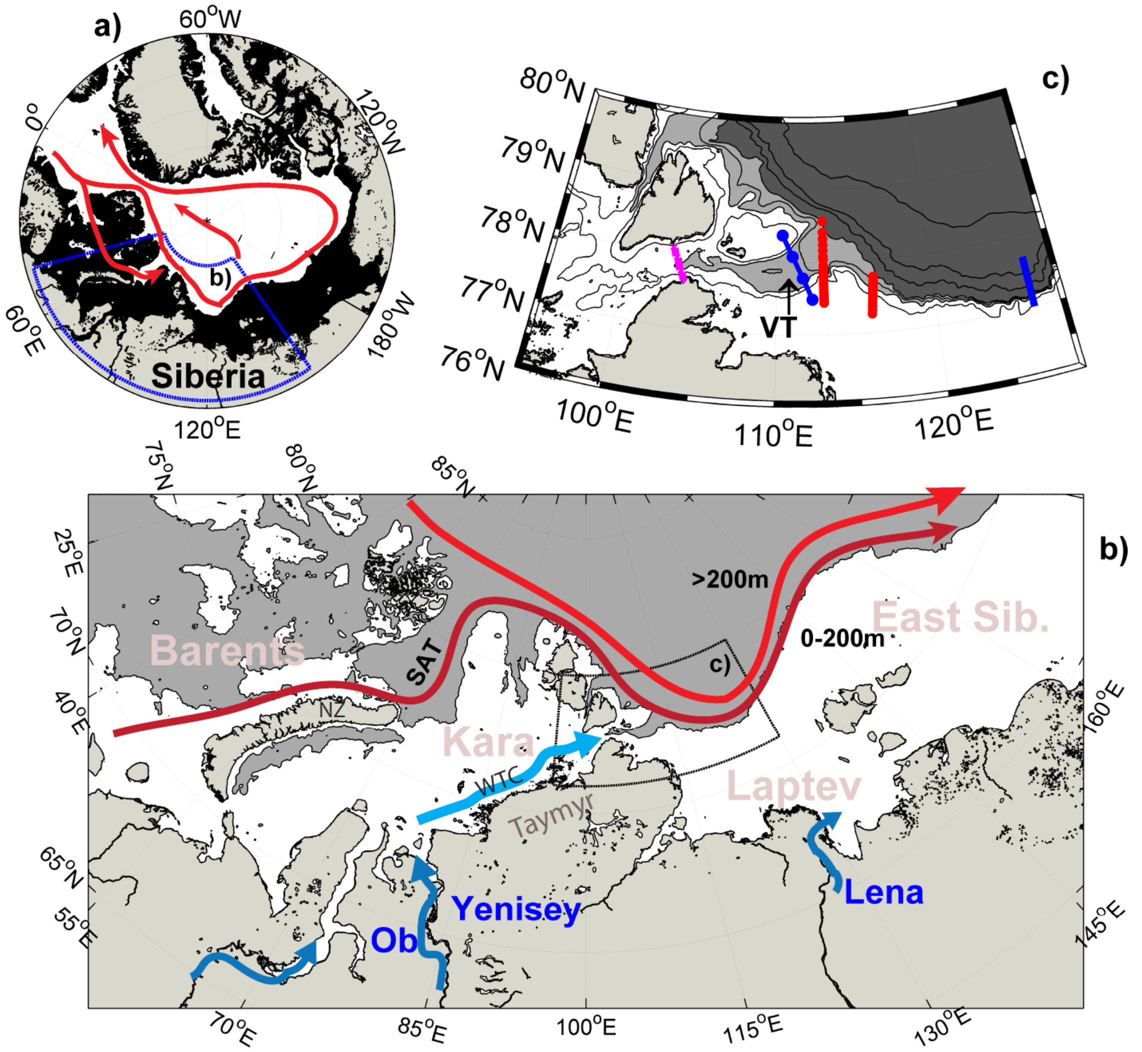

Figure 1: a) Map of the Arctic Ocean, the dark shading highlights the shallow shelf areas (<200 m), the box indicates the boundaries of panel b) map of the Kara and Laptev Seas region. Shading separates depths deeper (grey) and shallower (white) than 200 m from the International Bathymetric Chart of the Arctic Ocean (Jakobsson et al., 2008). c) zoom into the Vilkitsky Strait (VS) and Trough (VT) region. Colored lines and dots show transect locations: VS model-transect (magenta), *RV Polarstern* 2011 VT-transect (blue dots), 2013 UCTD-transect along 113°E and 116°E (red dots), and the 126°E-NABOS-transect (blue line).

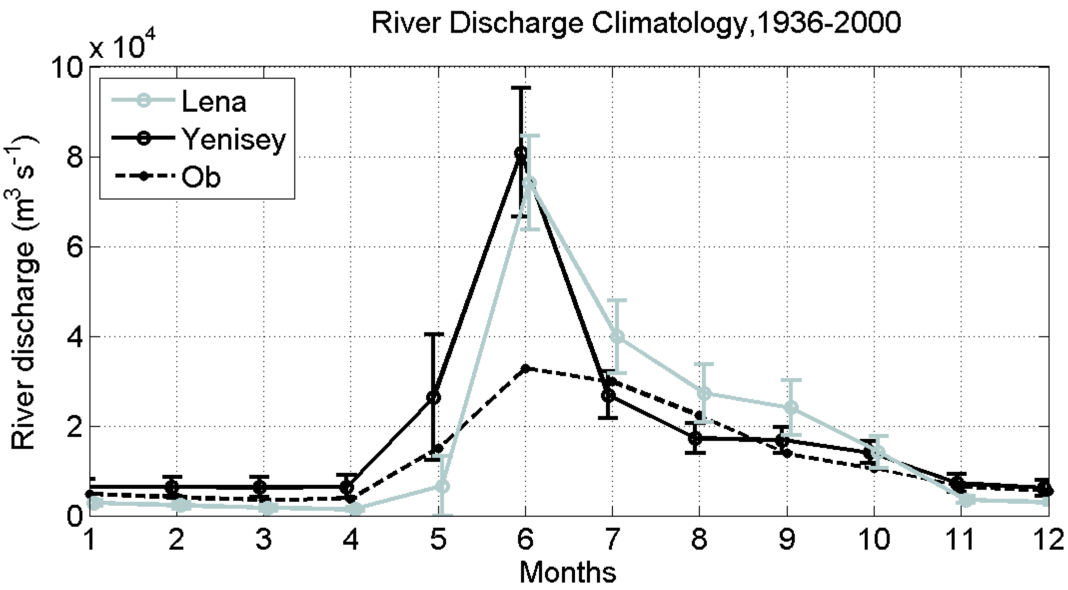

Figure 2: Monthly climatological river discharge rates (m^3 s^{-1}) from the three largest Siberian rivers, computed from ArcticRIMS runoff data from 1936-2000 including the standard deviations for Lena and Yenisey.

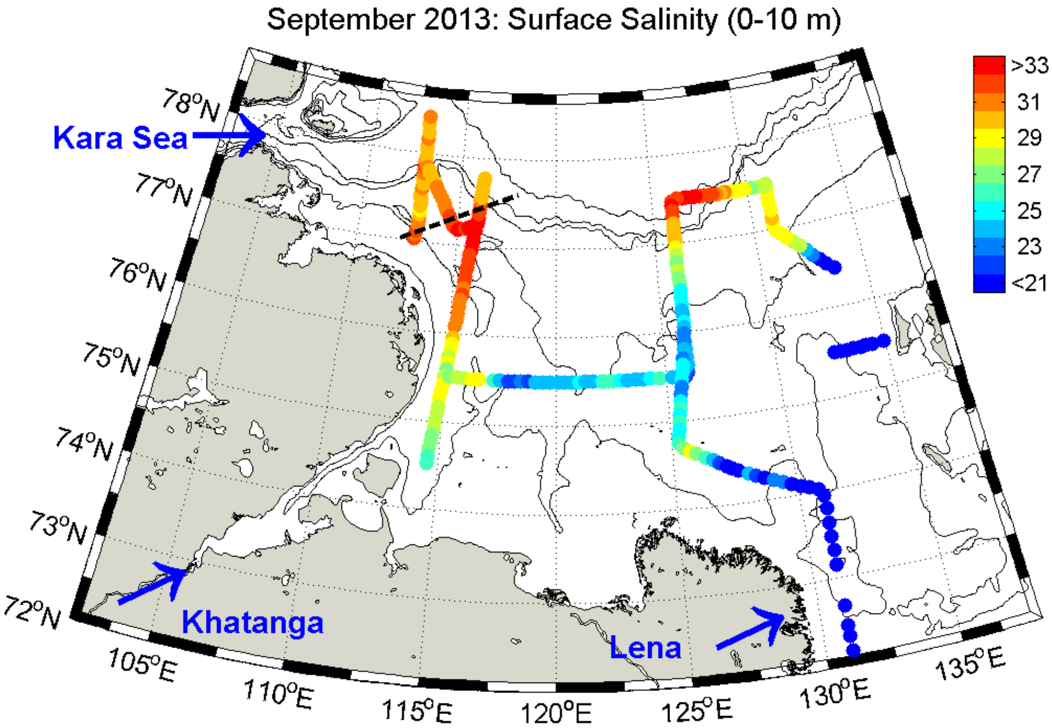

Figure 3: Mean surface (0-10 m) salinity in September 2013 sampled with an Underway CTD during Transdrift 21. Note that all salinity values are capped below 21 and above 33, minimum salinities were as low as 6 psu near the Lena Delta. The dominant freshwater sources are indicated with blue arrows (Lena and Khatanga Rivers, as well as the Kara Sea outflow). Depth contours show the 20 m, 50 m, 100 m, 200 m, and 1000 m isobaths. The dashed line in the northwest Laptev Sea indicates a boundary between Kara Sea waters in the northwest, and Lena waters based on salinity and neodymium measurements (G. Laukert, unpublished data).

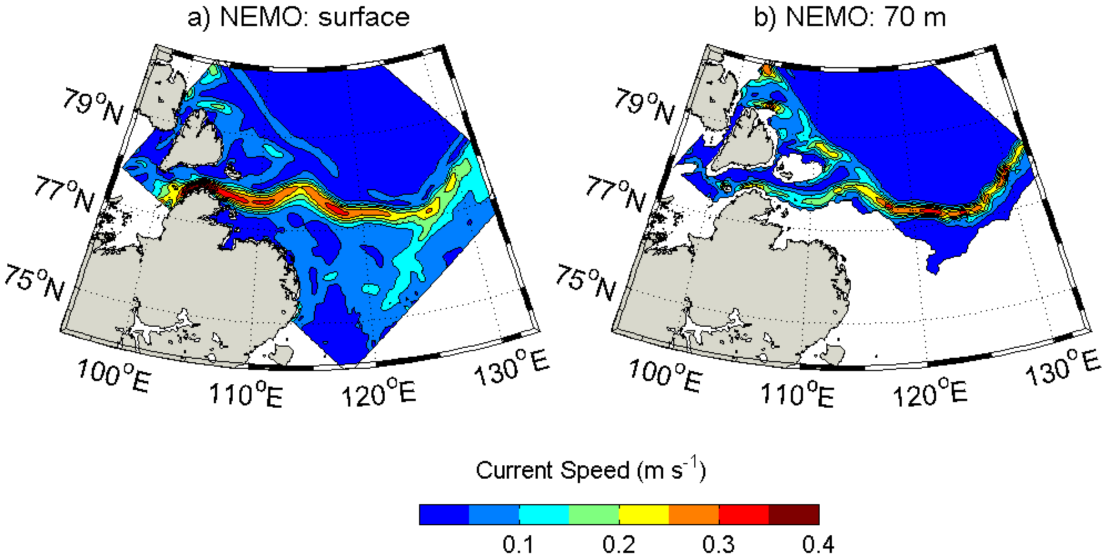

Figure 4: Mean (1990-2010) October a) surface and b) 70 m current speed from NEMO (m s^{-1}).

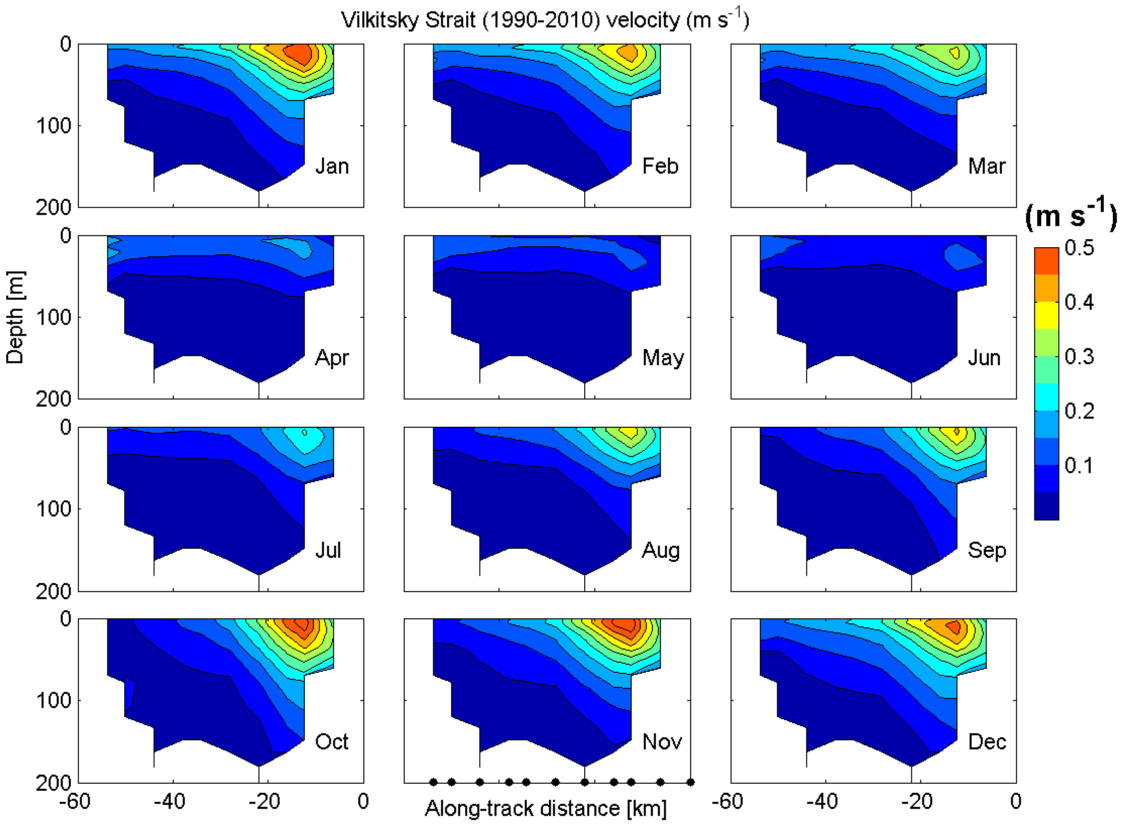

Figure 5: Monthly mean velocities across Vilkitsky Strait versus depth from NEMO (1990-2010). The right-hand of the transect (km 0) is the south side (i.e. the Laptev Sea side), flow toward the Laptev Sea is into the page. Black dots in November-panel indicate model grid points (see Figure 1 for location).

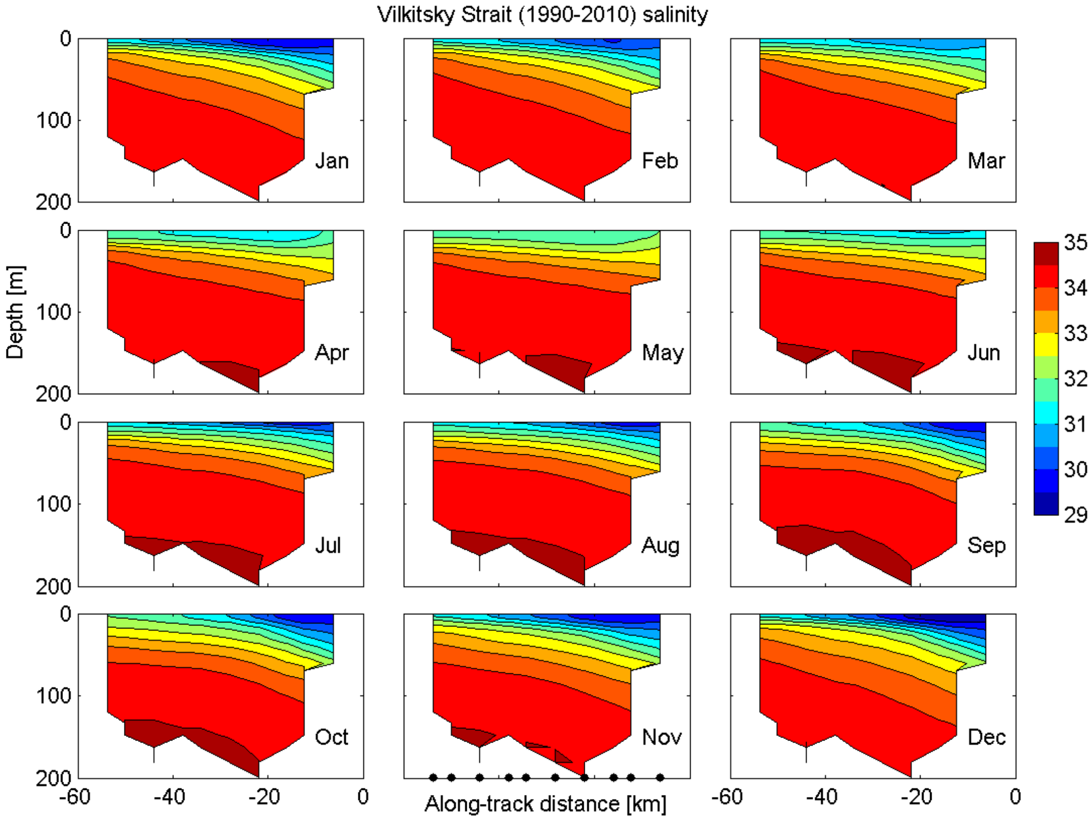

Figure 6: Same as Figure 5 except for salinity.

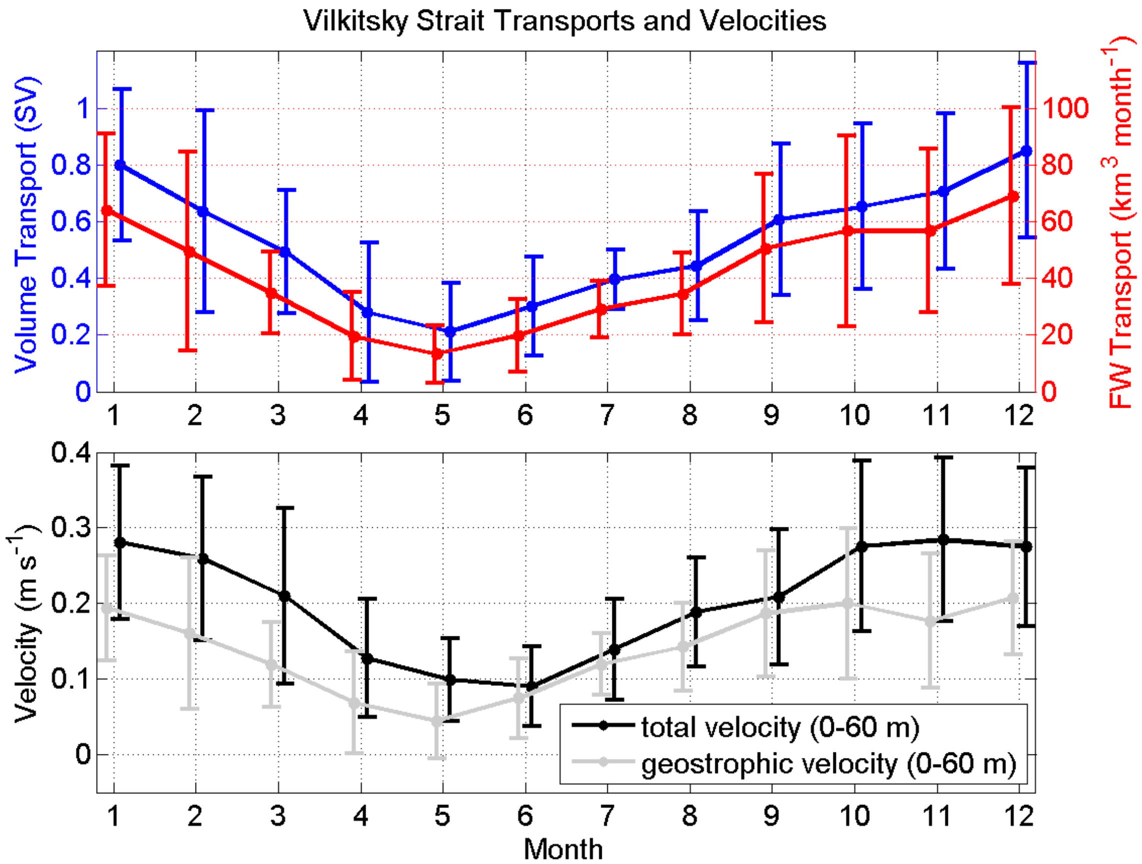

Figure 7: Monthly mean (top) volume (Sv) and freshwater (km^3 month^{-1}) transport through Vilkitsky Strait from NEMO (1990-2010) and (bottom) mean (0-60 m) total (black) and geostrophic velocities (grey) computed from the NEMO density structure. Vertical bars denote one standard deviation.

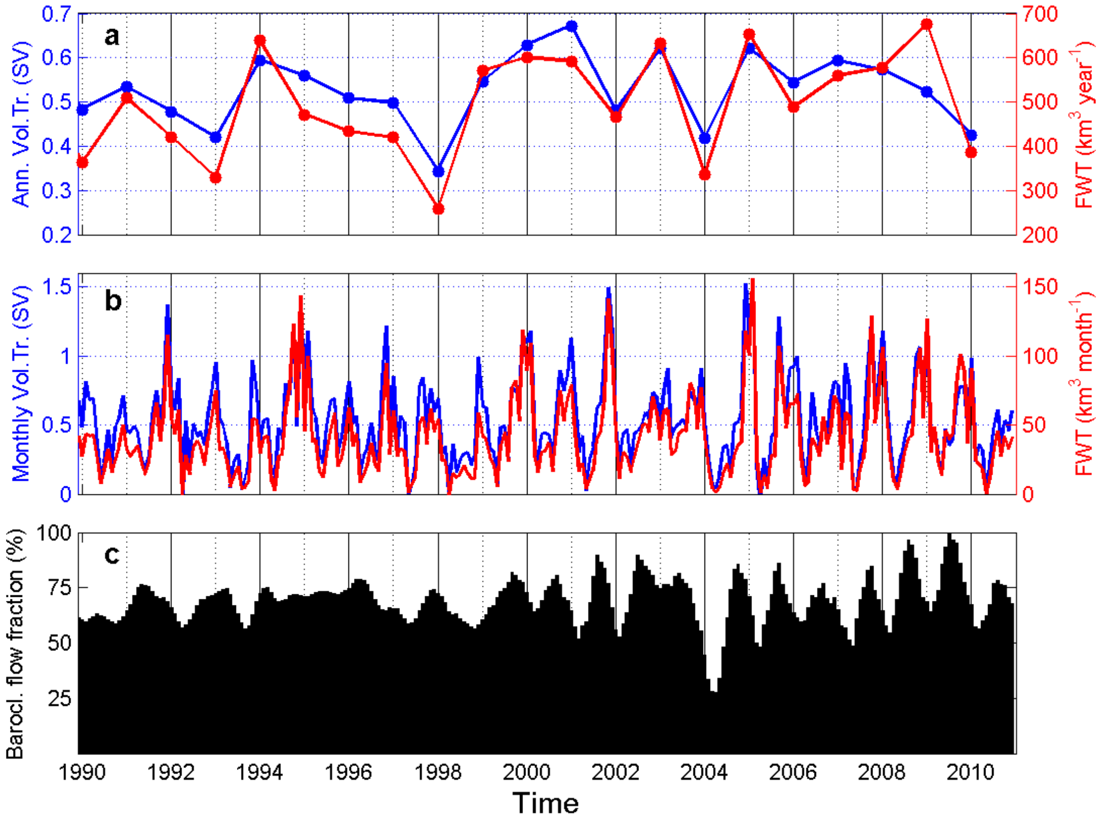

Figure 8: Model-based: (a) Annual means of volume (blue, [Sv]) and freshwater transport (red, [km^3 year^{-1}]). (b) monthly mean volume (blue) and freshwater (red) transports. (c) Baroclinic flow fraction in Vilkitsky Strait, i.e. the fraction of geostrophic vs. the total velocities in the upper 60 m. x-ticks mark January of each year.

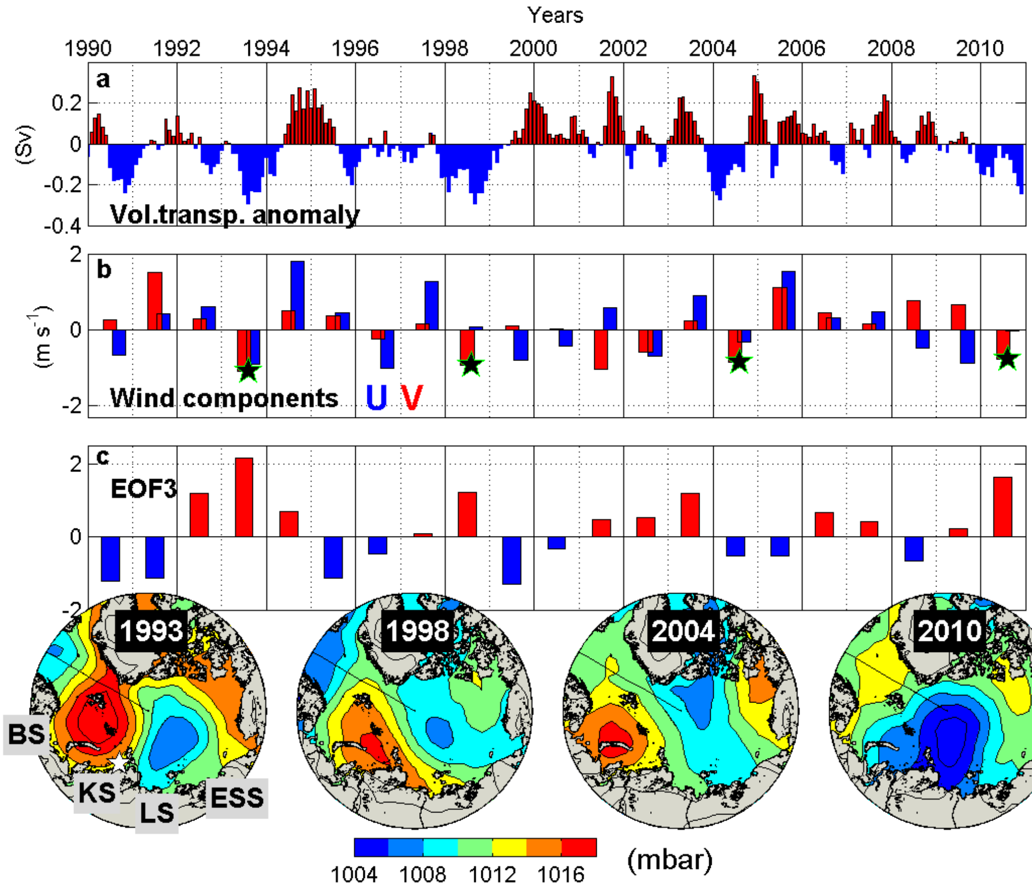

Figure 9: a) Volume transport anomaly through Vilkitsky Strait based on NEMO 1990-2010, x-ticks mark January of each year. (b) NCEP summer wind components over the eastern Kara Sea (white star in panel ”1993”, averaged from July-September. (c) principal components from the third leading EOF decomposed from JAS sea level pressure (60-90 °N). (d) Summer (JAS) SLP distribution during years characterized by strong negative transport anomalies through Vilkitsky Strait, indicated by green stars in the middle panel.

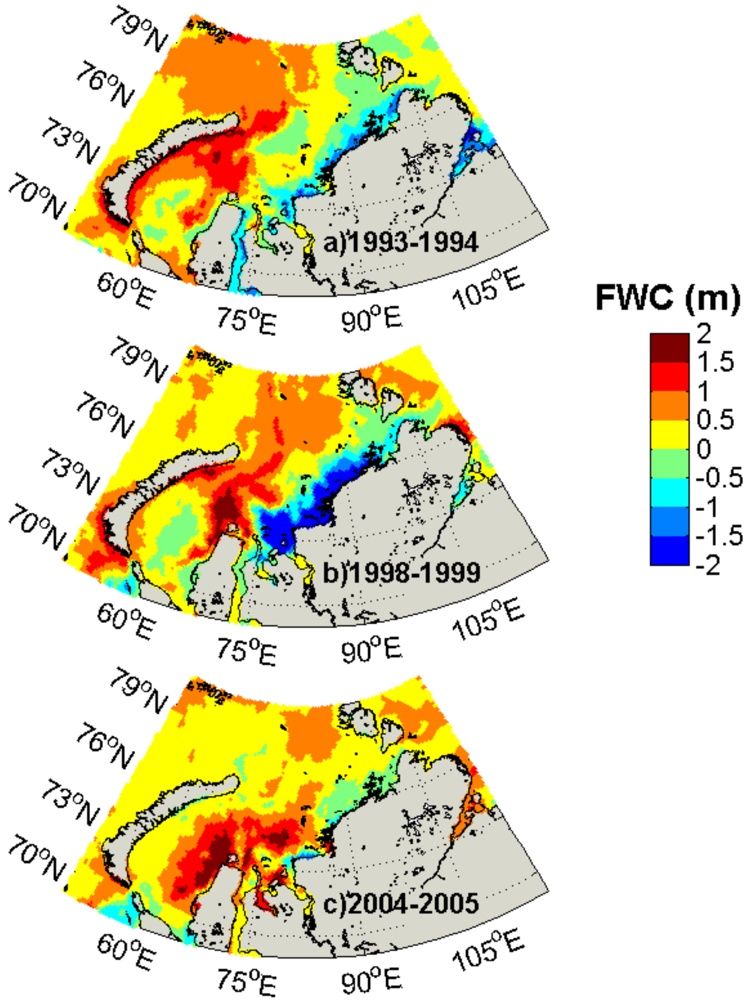

Figure 10: Maps of simulated Kara Sea freshwater content difference (m) between the summers of: a) 1993 minus 1994; b) 1998 minus 1999; and c) 2004 minus 2005.

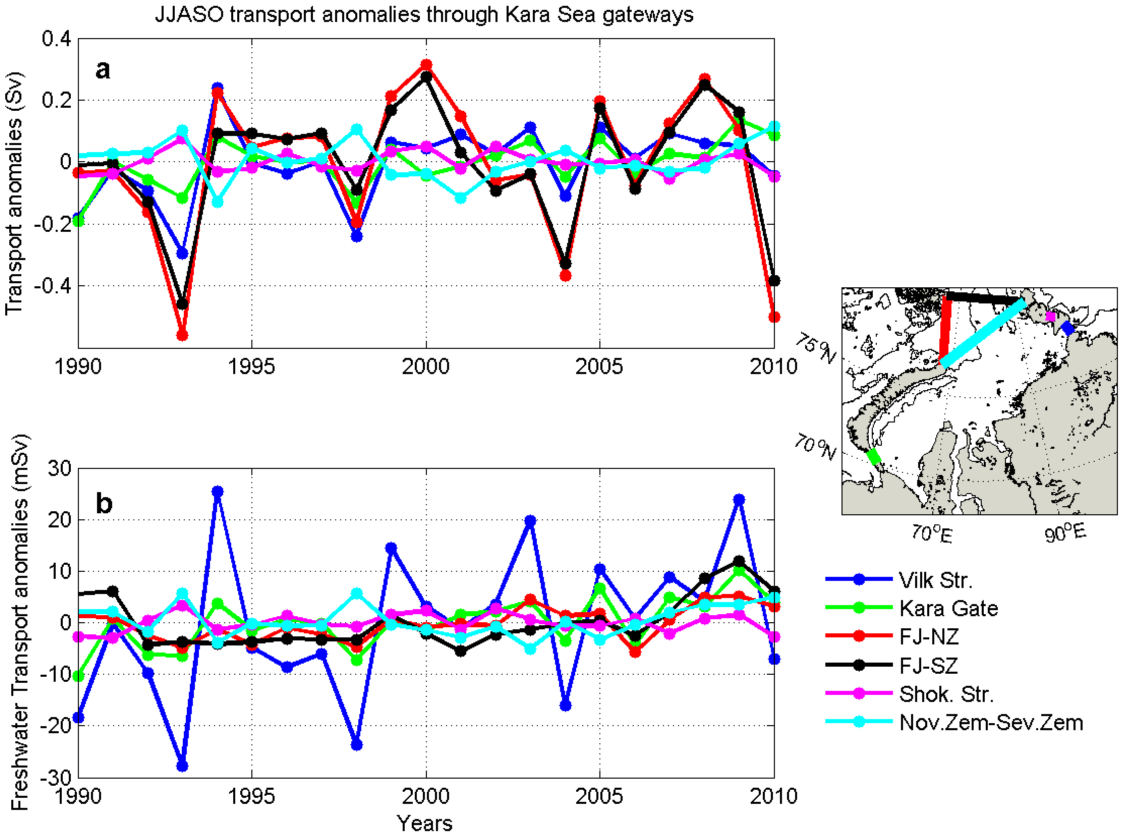

Figure 11: a) Volume (Sv) and b) freshwater (mSv) transport anomalies from NEMO computed from June-October averages across all major Kara Sea gateways. The colors indicate the boundaries as shown in the small map (blue: Vilkitsky Strait; green: Kara Gate; red: Franz Josef Land (FJL) to Novaya Zemlya (NZ); black: FJL to Severnaya Zemlya (SZ); magenta: Shokalsky Strait; cyan: NZ to SZ.

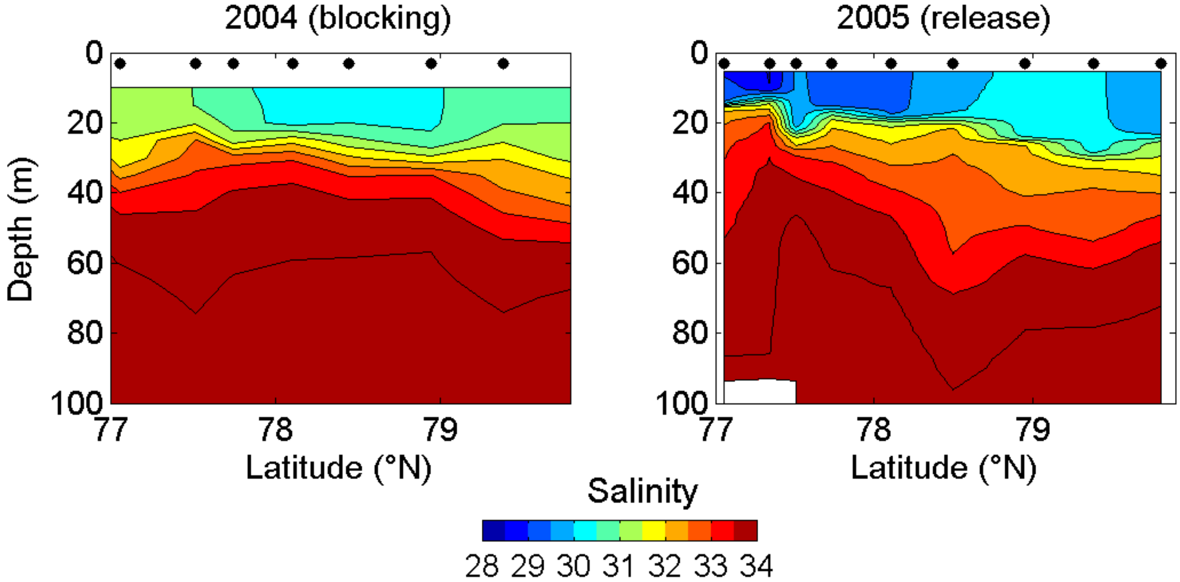

Figure 12: NABOS salinity transects along 126°E (see Figure 1 for location) during the summers of 2004 (left) and 2005 (right). Note the comparatively high salinity (low salinity) in 2004 (2005) during negative (positive) freshwater transport anomalies in Vilkitsky Strait.

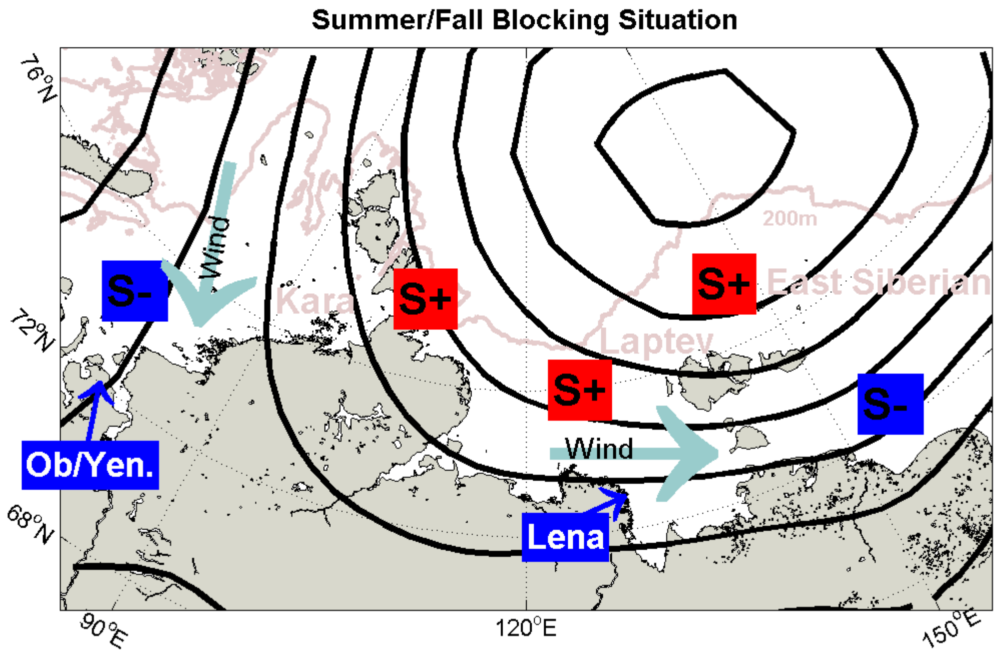

Figure 13: top) The black contours indicate the third largest mode of variability, based on an EOF analysis of Arctic Ocean (latitude >60°N) summer (JAS) NCEP sea level pressure from 1948-2013. This pattern corresponds to a blocking situation of the VSC due to onshore winds (indicated by arrows) over the eastern Kara Sea leading to negative anomalies in Vilkitsky Strait volume and freshwater transport. At the same time, winds are zonal over the southern Laptev Sea, leading to an eastward diversion of the Lena River plume. Overall, this situation leads to positive salinity anomalies in the Laptev Sea, as indicated by the red "S+" - boxes, and to negative salinity anomalies in the Kara and the East Siberian Seas.

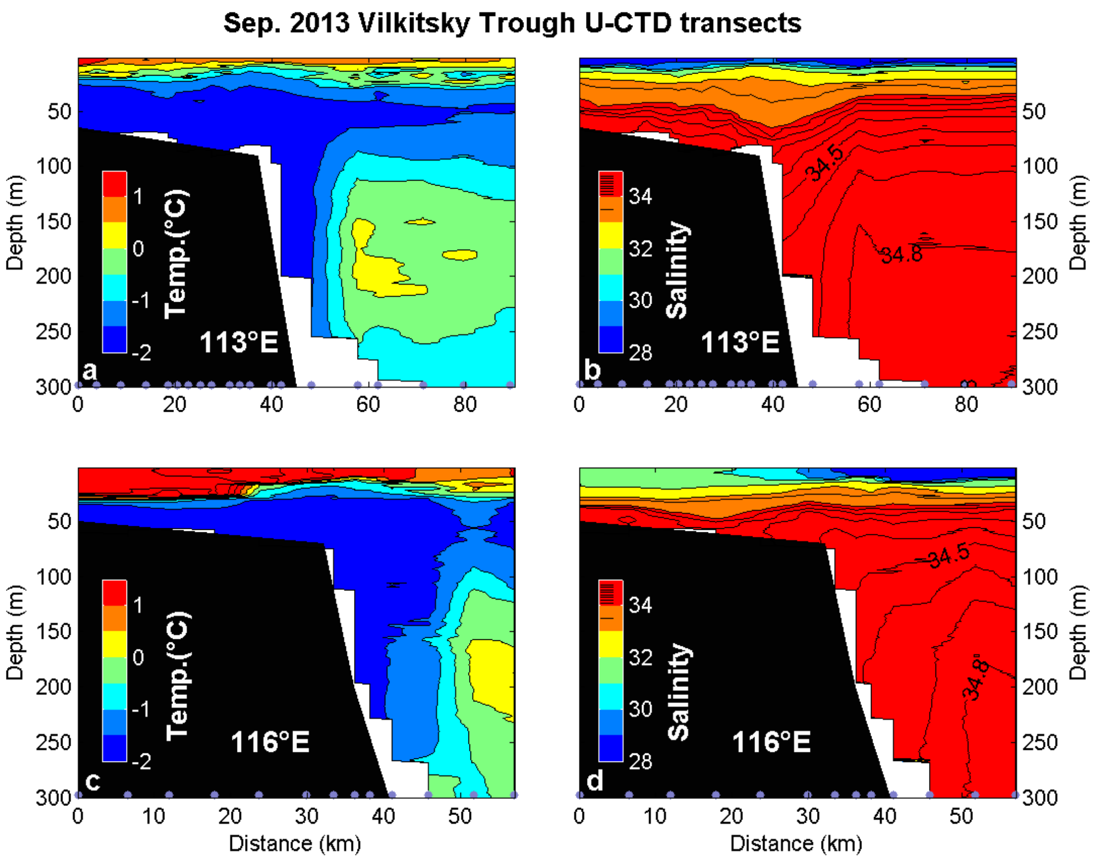

Figure 14: Cross-slope temperature (°C; a, c) and salinity (b, d) underway-CTD transects from September 2013 along 113°E (a, b) and 116°E (c, d) (see Figure 1 for location) vs. distance (km). Dots at the bottom of the panels indicate station locations.

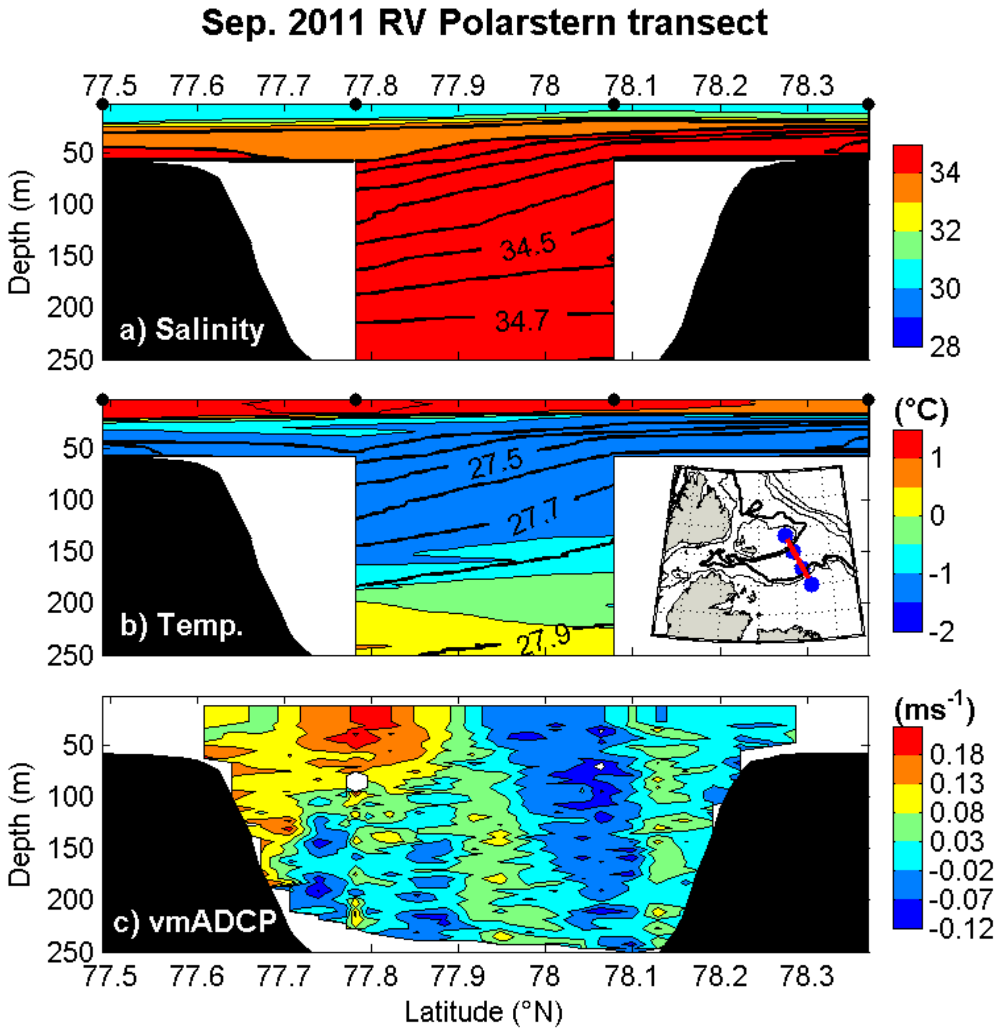

Figure 15: Cross-canyon CTD and vmADCP transect carried out by *RV Polarstern* in September 2011. a) salinity, b) temperature (°C) overlaid by density contours (kg m^{-3}), c) vessel-mounted ADCP velocity (ms^{-1}, positive eastward); small insert map in b) shows the location of CTD stations (blue dots) and ADCP transect (red line). Black dots in a) and b) indicate station locations. The black shading indicates the along-track bottom topography, extracted from IBCAO (Jakobbson et al., 2008).

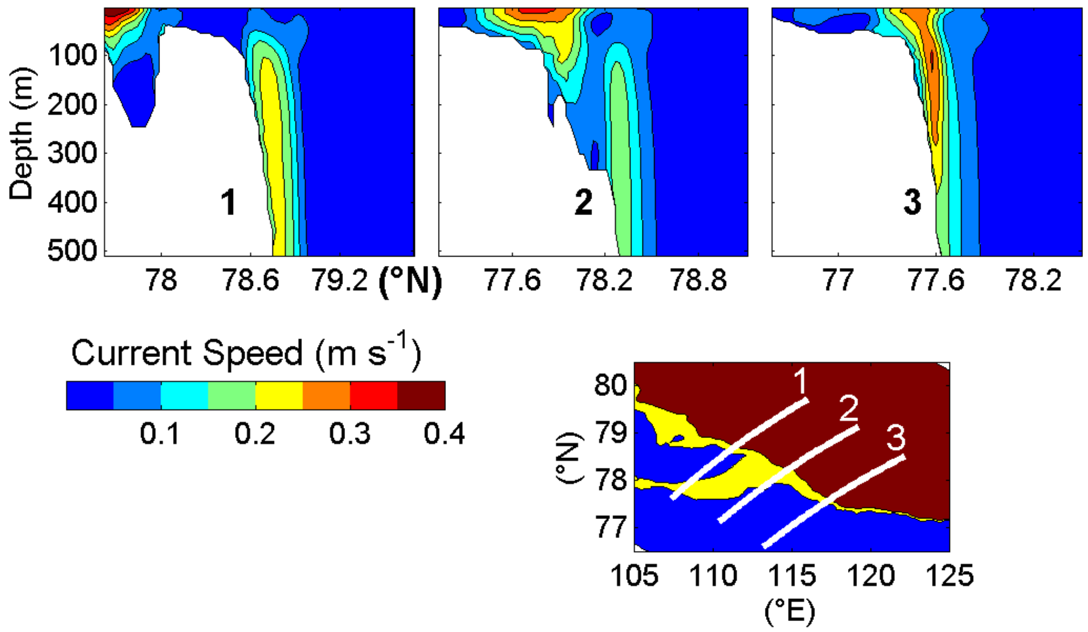

Figure 16: Current speed (m s^{-1}) in three model-based example transects from January 2004 showing the merging of the Barents Sea branch with the Vilkitsky Strait Current. Lower panel shows the location of the three transects.